EFFECTIVE THERMAL CONDUCTIVITY OF POROUS MATERIALS USING MAXWELL'S METHODOLOGY AND IMAGE-BASED FINITE ELEMENT APPROACH

by

Vrushank Deepak Balutkar

A thesis submitted to the faculty of
The University of North Carolina at Charlotte
in partial fulfillment of the requirements
for the degree of Master of Science in
Mechanical Engineering

Charlotte

2020

Approved by:

Dr. Harish P. Cherukuri

Dr. Gloria Elliott

Dr. Ahmed El-Ghannam

ABSTRACT

VRUSHANK DEEPAK BALUTKAR. Effective Thermal Conductivity of Porous Materials using Maxwell's Methodology and Image-Based Finite Element Approach. (Under the direction of DR. HARISH P. CHERUKURI)

The steady-state thermal response of solid materials is controlled by their thermal conductivity. For porous materials, the local thermal conductivity is difficult to use in the characterization of the overall thermal response and therefore, often, the concept of effective thermal conductivity that depends on the porosity is used. In this work, two methods for computing the effective thermal conductivity of porous materials are studied. The first approach uses an image-based approach where a stack of 2-dimensional images are used to build a three-dimensional structure with porosities. The effective thermal conductivity of this structure is then calculated using the finite element software ABAQUS. The second approach, known as Maxwell's method, is used on a medium consisting of spherical pores arranged in various configurations such as simple-cubic, body-centered cubic and face-centered cubic arrays. Results from the numerical simulations and the applicability of the two approaches to structures with complex porous structure are discussed. The effect of porosity on the effective thermal conductivity is also discussed.

DEDICATION

To my parents, Mr. Deepak Balutkar and Mrs. Sushama Balutkar

And

My brother, Mr. Chinmay Balutkar

ACKNOWLEDGEMENTS

I would like to thank my research advisor and Department Chair of Mechanical Engineering and Engineering Science of UNC Charlotte, Dr. Harish Cherukuri for providing his guidance and expertise throughout my research. I am also thankful to my committee members, Dr. Gloria Elliott and Dr. Ahmed El-Ghannam for their valuable time and guidance. I would like to thank my family for their moral and financial support. I would also like to acknowledge Swapnil Bansode, Sudeep Agalgaonkar, Sarvesh Mehendale and Mouli Chattaraj for their help in this research. At last, I am grateful to all the faculty and staff members here at UNC Charlotte.

TABLE OF CONTENTS

LIST OF TABLES

LIST OF FIGURES

LIST OF ABBREVIATIONS

DIB Digital Imaged-Based

FEA Finite Element Analysis

OOF3D Object Oriented Finite Element Three Dimensional

RVE Representative Volume Element

TBC Thermal Barrier Coatings

CHAPTER 1: INTRODUCTION

The Fourier' law of heat conduction relates heat flow and temperature field gradient through the relationship

$$q''(\hat{r}, t) = -k\nabla T(\hat{r}, t), \tag{1.1}$$

where $q''(\hat{r}, t)$ is the heat flux vector, ∇T is temperature gradient, $\hat{r}$ is the position vector, t is time and k is thermal conductivity. For a given temperature gradient, the flow of heat is directly proportional to thermal conductivity of a material [2]. From the Fourier law, the units for k are easily deduced as $W/(m.K)$. Furthermore, k can also be defined as the amount of heat flowing through a material per unit time through unit area as a result of unit temperature gradient. If the solid medium through which heat energy is conducted has inhomogeneities or pores, the heat transfer is affected and the heat energy changes. In this case, the concept of effective thermal conductivity is used in designing and selection of materials for different engineering applications. For example, porous ceramics have a wide range of applications in sensors, ceramic filters, bio-materials, catalyst carrier, porous electrodes, thermal barrier coatings and so on [3]. Thermal Barrier Coatings (TBC) are used to protect and insulate hot-section metal components in diesel engines and advanced gas turbines where temperature reduction up to 200°C can be obtained, which in turn improves and enhances the metal component [4]. Effective thermal dissipation is used in several energy systems and electronic systems such as LED, Li-ion battery, solar cells and micro electric packaging. These applications have composites porous materials and thus it is important to evaluate their effective thermal conductivity. Of the several methods available to calculate effective thermal conductivity, two are considered

in this study. One is an image-based finite element analysis (FEA) of multi-phase materials. Second, Maxwell's methodology applied to thermal analysis for periodic spherical pores and spherical and cubical effective medium. The image based FEA can be used to calculate effective thermal conductivity for any porous material with random or periodic pore structures. In this method, a cross sectional image of said porous material is captured and several such images are combined to create a three dimensional model. Object Oriented Finite (OOF) elements software application is used for studying the microstructure of porous materials and its response to thermal properties [5]. The other method for estimating effective properties of materials, derived by Maxwell (1873), aided in approximating electrical conductivity of a particle cluster by looking at the effect of the cluster on the far-field when the system is subjected to a uniform electric field. This method has been extended to thermal conduction problems with pores of different sizes and structure [6].

1.1 Thesis Objective

The objective of this thesis is to study the effective thermal conductivity of porous materials using two methods as discussed above. In the image-based finite element analysis, a three dimensional model of a micro-structure with random distribution of pores is considered. In the Maxwell's methodology for thermal problems, a matrix embedded with spherical pores along with spherical and cubical effective media are considered. Effective thermal conductivity is assigned to the spherical and cubical effective media, where the temperature distributions are plotted and compared. The effects of porosity, pore distribution and pore geometry on the effective thermal conductivity are studied as well.

1.2 Thesis Outline

The rest of the thesis is organized as follows.

Chapter 2 discusses different numerical methods used to calculate effective thermal

conductivity. The porosity of different composites affect their effective thermal conductivity and thus is an important factor. We use a representative volume element for digital image-based FEA and apply Maxwell's methodology using FEA.

Chapter 3 studies Image-based FEA used for microstructures with pores of various spatial arrangement and sizes, detailed explanation of which have been provided. Random porous microstructure images are stacked and a three dimensional model is generated. OOF3D is used to mesh and assign material properties to the different phases and it is then imported into ABAQUS for thermal analysis.

Chapter 4 explores the application of FEA in calculating effective thermal conductivity using Maxwell's methodology. Three types of structures are used to arrange pores in a cubical array. Both spherical and cubical inhomogeneities are used as effective media. Thermal boundary conditions are applied across the top and bottom surface of the matrix encompassing both pores and the effective medium.

Chapter 5 discusses the effect of porosity on effective thermal conductivity. Three different pore structures and arrangements are presented.

Chapter 6 includes results of FEA using both image-based process and Maxwell's methodology. Linear regression plots between porosity and effective thermal conductivity are also shown in this chapter.

In Chapter 7, conclusions are derived from the results obtained by comparing all the structures and both effective medium. Future work is also presented.

CHAPTER 2: LITERATURE REVIEW

Thermal conductivity is an important parameter for heat conduction; the heat flux is directly dependent on the former through Fourier's law. Thermal conductivity varies with materials and their state. For example, solids have higher thermal conductivity than most liquids and gases. There is variation of thermal conductivity due to change in temperature and it can also have directional dependence as in anisotropic materials [2]. For inhomogeneous materials and composite materials, it can vary from point to point.

Composite materials with multiple phases or different material properties for different phases are modeled as homogeneous materials having effective properties [7]. Thus we can define effective thermal conductivity as the average thermal conductivity of a composite material with different phases or pores, which can be determined by using steady-state thermal analysis.

The concept of Representative Volume Element (RVE) is usually used to numerically determine properties of composite materials. For this, the pore distribution should be isolated and correct boundary conditions are to be applied on the RVE so as to obtain results similar to real structure. RVE is a unit cell that can be isolated from a composite material as the material as a whole consists of random distribution of pores across the cross-section. Hence, for simplicity, the models assume an RVE which is isolated having the same material constants [7]. In this paper, the average stress and strain quantities are defined to confirm the equivalence between the original heterogeneous material and its analogous homogeneous material. In another paper, square RVE and cylindrical RVE are studied and the effective mechanical properties of carbon nano tube (CNT) are calculated using FEM [8].

To calculate effective thermal conductivity we consider a cross-section of a material with pores. The top and bottom surfaces are prescribed with fixed temperature conditions T_1 and T_2. The side surfaces are considered as insulated ($Q = 0$), where Q is the heat flux. Thus through Fourier's law we can determine the effective thermal conductivity as

$$k_{eff} = \frac{QL}{W\Delta T} \tag{2.1}$$

where, k_{eff} is effective thermal conductivity, L is the height and W width of the the model, Q is the steady state heat flux and ΔT is the temperature difference between bottom and top boundaries [9].

The effective thermal conductivity of porous materials is influenced by the size and structure of pores [3]. The effects of pores and interfaces are studied by Z.Wang et al. for plasma sprayed zirconia coatings. The paper studies two different approaches to observe the effect of pores on the operative properties of the material. In one approach, Small-Angle Neutron Scattering (SANS) studies are conducted to quantify the micro-structure of zirconia coatings. In this method, an artificial rebuilding of the porous material is carried out. The other approach uses microstructural images obtained from Scanning Electron Microscope (SEM). A model is constructed by thresholding these images by using OOF3D. The effective thermal conductivity is calculated using similar methods as described above. There are two important factors to be considered while modelling the porous materials. First, the model should be large so that it contains enough features of the microstructure so as to obtain a representative thermal or mechanical response. Second, all the details of the microstructure should be involved so that it is similar to the real microstructure [9].

Modelling RVE for the microstructure of a composite material with different shapes and sizes of pores is very difficult. The geometric information about the composite material or microstructure can be obtained through a set of cross-sectional images. Image processing and digitizing the pixel and voxel is done to create a FE model.

Digital Imaged Based FE modelling can be used to automatically generate the FE model accompanied with homogenisation method for predicting thermal and mechanical behaviors of the microstructure.

The process of digital imaging of microstructure involves capturing the image and sampling it into numerical form. Then a unit cell is selected from the microstructural image followed by observing the pixel distribution, and a gray scale image is constructed using thresholding operation. A threshold value is decided below which the value of the pixel becomes 1 and above which it becomes 0. Resolution of the image is adjusted accordingly to obtain perfect boundaries between the phases. Several images, after going through the similar process are stacked to create a FE model. After the model is generated, it is used for finite element analysis [10] [11].

In this research, Object Oriented Finite Elements in three dimension (OOF3D) is used for the digital image based finite element analysis. It provides all the procedures described above and can also be used for meshing the geometric model and solving Partial Derivative Equations (PDE) using finite element models. The software has a Graphic User Interface (GUI) for visualising the microstructure in 3D. It uses several options including snap nodes, smoothing boundaries, rationalizing shapes and refining all elements [5]. The design of the OOF code is explained and formulated by Patzak and Bittnar in their paper [12]. Chawla et al. [13] have used this technique for thermo-mechanical simulation, whereas Takano et al. [14] have used similar techniques for utilizing homogenization method.

Similar methods are used in many applications like Al open-cell foam where the specimen is ground and polished in order to capture its cross section [15]. Three dimensional RVEs are generated by Sharma et al. [16] in their paper for densely packed Al/SiC composites for modelling thermal expansion.

Celik et al. [17] study the effects of residual stresses in plasma sprayed MgO-ZrO_2 coatings for internal combustion diesel engine. The percentage of porosity influences

the level of thermal stresses in the coatings which are subjected to thermal shock. In this study both thermal and structural FEM were used to investigate the effects. A two dimensional model was created with fine mesh.

Thermal conductivity can also be calculated by considering the theory of scattering phonons by point defects and hopping of oxygen vacancies. The thermal conductivity of Yttria-Stabilized Zirconia (YSZ) ceramic is measured using this theory [4]. Increase of effective thermal conductivity due to radiation at high temperature is also considered in aforementioned theory. The models were generated using the SEM images of the cross-section of YSZ and the pores were measured using ContextVision image analysis software. Maxwell's theory was applied in this study as well.

In their paper, Anish K. John et al. [18] use a numerical method to determine the effective thermal conductivity of heat exchanger surfaces. The heat exchanger has a perforated plate matrix through which conduction occurs. The effective thermal properties of the perforated heat exchanger plates are obtained using ANSYS software. In this paper, the porosity and perforation factor effects are studied, which is the ratio between the perimeter of perforation to the plate thickness. The temperature is determined using steady state thermal analysis, neglecting the radiation effects. The perforated plate is modeled in a rectangular structure, and conduction and convection conditions are applied. Material properties of copper, like density, thermal conductivity and heat capacity are used. Constant heat flux is applied on two opposite boundaries of the rectangular structure and the other boundaries are considered adiabatic.

Various insulating media are also considered as multi-phase materials. They contain numerous voids which affect the thermal conductivity of the medium. A 3D printer can be used to generate samples with pores of different shapes and sizes to investigate their thermal properties. In their paper, Chung et al. [19] use a series of samples with different anisotropic void distributions generated using 3D printing . In that

the sample is created in any CAD software and converted into the required data description for the 3D printer. The sample quality is also confirmed using X-ray to check the anisotropic voids. A hot disk device sensor is used to determine the thermal properties of the samples and the effects of the void on them; FE simulations are also conducted on the samples for the study. The void alignment and distribution strongly affects the material response.

Maxwell's far-field methodology for predicting effective electrical conductivity, was adapted into an analogous process to derive effective thermal conductivity. The methodology is analogous to thermal problems and hence can be used to determine effective thermal conductivity. In the paper [6], it is shown that the methodology is not restricted to low volume fractions, which was originally suggested by Maxwell. The methodology can also be used to determine effective elastic properties [20] [21].

In this methodology, two cases are considered. The first case consists of a cluster of N types of particles embedded and bonded in an infinite matrix. The radius of those particles is $a_i, i = 1, 2, .., N$. The superscript i is used to denote the particles with different properties. These particles are enclosed in a sphere of radius b. Volume fraction is considered for this derivation. The volume fraction of a composite can be defined as the ratio of volume of different materials present in the composite over the volume of the whole composite. Volume fraction of the particles in the matrix is given as:

$$V_p^i = n_i a_i^3 / b \;\text{ such that } V_m + \sum_{i=1}^{N} V_p^i = 1. \tag{2.2}$$

In the second case an isolated sphere is embedded in an infinite matrix. At large distance, the cluster can be considered as a single point at the center. Thus at large distances from the cluster and the effective medium the temperature distributions should be identical [6]. After equating the perturbance and solving we get the effective

thermal conductivity as:

$$k_{eff} = V_p K_p + V_m K_m - \frac{(K_p - K_m)^2 V_p V_m}{V_p K_m + V_m K_p + 2K_m}. \tag{2.3}$$

For evaluating the effective thermal conductivity of isotropic materials, a numerical technique based on Maxwell's methodology is presented by Olesya Koroteeva et al. [22] in their paper.

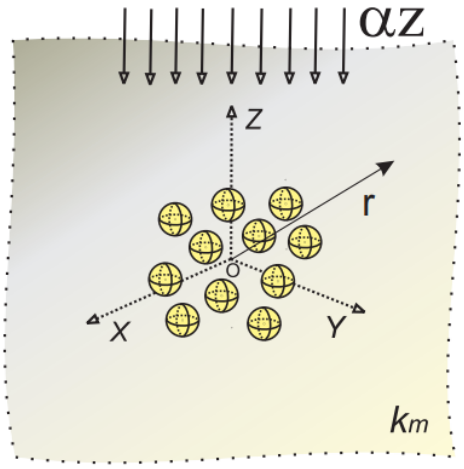

Figure 2.1: Cluster of spherical particles embedded in infinite matrix [1]

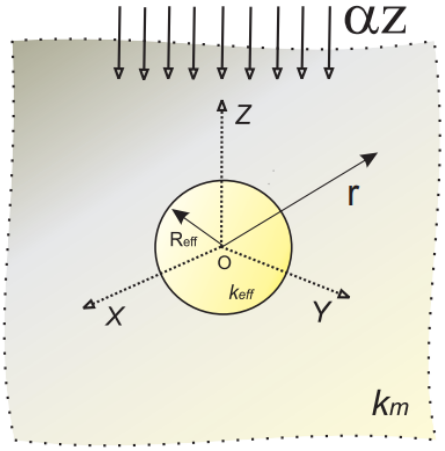

Figure 2.2: Spherical effective medium embedded in infinite matrix [1]

The pores considered in the material are of periodic or random arrangement. The technique uses clusters of spherical particles and a spherical effective medium in an infinite matrix. The temperature at distant points from the cluster and the spherical effective medium is the same. Thus the effective thermal conductivity is defined by the thermal properties of the effective medium [22]. Effective thermal conductivity is also calculated using equivalent homogeneity method by accounting the interactions between the spherical particles in the cluster. This approach is the extension of Maxwell's methodology and predicts the effective thermal conductivity for low volume fractions [1]. Another modification to this method can be employed by using cubic equivalent inhomogeneity or cubic effective medium instead of spherical effective medium. The results for cubical inhomogeneity converge to the benchmark solutions [23]. Maxwell's methodology can also be combined with boundary element method to obtain the effective properties of composite materials with non-spherical pores [24].

CHAPTER 3: IMAGE-BASED FINITE ELEMENT ANALYSIS

Composite materials with multiple phases have various implementations. The thermal analysis of the composites is essential for many engineering applications. The material properties change due to inhomogeneities present in the microstructures of the composite materials. Hence, effective thermal conductivity is an important parameter used for the selection of materials for different practices.

For accurate prediction of the material properties both destructive and non-destructive methods can be used. The non-destructive methods have advantages over the destructive ones due to their feasibility and economic benefits. Both elastic and thermal properties can be assessed with these methods. One of these include the use of micro-computed tomography (micro-CT) to capture images of microstructure in order to generate a computational model [25]

Digital image-based approach can also be used for calculating material properties and generating material models. The composite materials have periodic or random distribution of the multiple phases. Spatial and orientation information is necessary to generate accurate models of the material in consideration. Representative Volume Element (RVE) is used to determine these properties and model generation. An RVE is assumed for the corresponding pore distribution to model different load distributions or boundary conditions [7].

It is difficult to assert a structure-property relationship in composites with random pore distributions. Thus model generation is a cumbersome task. Image-based model generation is an easy way to establish the relationship and conduct finite element analysis on the microstructural designs. Object oriented finite element technique is used to incorporate the microstructure for simulating the same. A three dimensional

model is generated by OOF3D software application by NIST. This is done by stacking multiple cross-sectional images of the microstructure to obtain the spatial distribution of pores.

A typical image-based FEA process involves multiple steps. The cross-section of the composite materials to be investigated is polished for smoother surface, important for capturing the microstructure. Polishing takes a very long time. The material surface is buffed and an image is captured; some more sections of the material with specific thicknesses is removed by polishing and is observed again. To obtain accuracy and continuity in the construction of a three-dimensional model, it is necessary that the specimen be captured at the same location [15]. The images can be photographed by using different sensors. These are usually optical devices such as Scanning Electron Microscope (SEM), Charged Coupled Device (CCD) camera, Stereoscopic microscope, and micro-CT scanners [10][14][15].

Image processing is carried out for the distinction of different phases in microstructure. The image goes through segmentation and smoothing. In this process, the image is converted into gray scale and the aim is to separate phases having different physical properties. Many image related changes are introduced in this process to smoothen the boundaries between the phases so as to obtain the accurate voxels required for meshing. The image resolution is adjusted so as to get the difference. The voxel element size is equal to the resolution of the image. A high resolution image increases the accuracy, but also increases number of voxel elements which requires higher computational power.

Material properties are assigned to different phases after smoothing out the interfaces. The gray scale image helps in identifying all the phases present in the composite material. This process has a demerit where the accuracy of the numerical results are bad at the phase interface [14]. These processes are carried out for multiple images of the composite material. These images are then stacked for a three dimensional

model. Thus we get a three dimensional microstructure of a composite material.

3.1 Example of microstructural simulation using OOF3D

OOF3D software application is used to apply the OOF technique to a random image as shown in the figure. OOF3D generates finite element mesh from two dimensional

Figure 3.1: Sample cross-sectional image of a microstructure

images or micro graphs. Mesh generation involves numerically feeding the straight lines, curves or planes. For microstructures, cubic element can be defined for every voxel. But this method has two demerits, one is that it create several elements to adequately describe the homogeneous regions and second, the interface between the phases are jagged which may result in stress concentrations [5].

OOF3D solves all these problems by using image-based adaptive meshing technique. This software application has several modules which aid in image processing, mesh generation and analytical solving. Digital images are arrays of voxels. These voxels are assigned material properties. The images are uploaded in the software and are stacked automatically to create a three dimensional microstructure.

The microstructure is then modified for resolution in order to obtain the specific number of voxel element to decide the computational requirements. The micro graphs

shows several pores randomly scattered. The boundary between the pores and the material is blurry. Using the image manipulation tools these pores are discerned from the material. It is first converted into gray scale and contrast image is obtained where two different phases can be easily identified.

The identified voxels are then categorised and a specific color is chosen to select voxels within the color range. Two voxel groups are established by this process, one for the material and one for pores. Material properties like thermal conductivity are assigned to the voxel groups. These properties are stored for every voxel of each phase. The next step involves creating a skeleton. A skeleton is the geometric representation of the finite element mesh to establish all the nodes and element edges. A skeleton is created so that it can be adapted to material boundaries. OOF3D only creates tetrahedral skeleton elements. The skeleton is made as homogeneous as possible by using skeleton modification tools. The largest fraction of an element's volume which belongs to a single voxel is called homogeneity. The skeleton is refined so that the homogeneity index approaches 1. To avoid jagged voxel boundaries we use different methods like Snap nodes, Anneal, Smooth. Snap nodes moves nodes to the intersection between materials. Anneal is used to randomly move nodes to beneficial points. Smooth option is used to move nodes to the average positions of the adjacent nodes. In OOF3D two terms are defined for modification of the

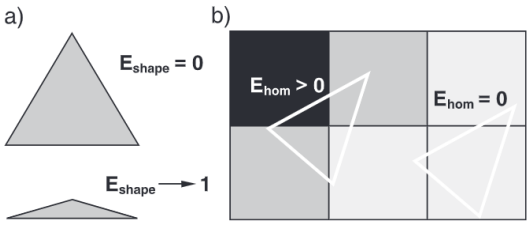

Figure 3.2: OOF3D Energy for meshing

mesh. The homogeneity energy is used to measure the match between the voxel and mesh and the shape energy is used to determine the quality of element shapes. The

anneal option treats the nodes as physical particles with energy and thus moves them accordingly. A good mesh can be defined when the weighted average of both energies when summed over elements is low. Homogeneity can be given as:

$$H = \frac{\max_i v_i}{V} \tag{3.1}$$

where, v_i is the volume within the element that belongs to the material i and V is the total volume of the element. Rationalize option is used to identify badly shaped elements which are then modified to increase homogeneity index. The next steps involve creating skeleton boundaries and finally meshing the microstructure. The skeleton is shown below.

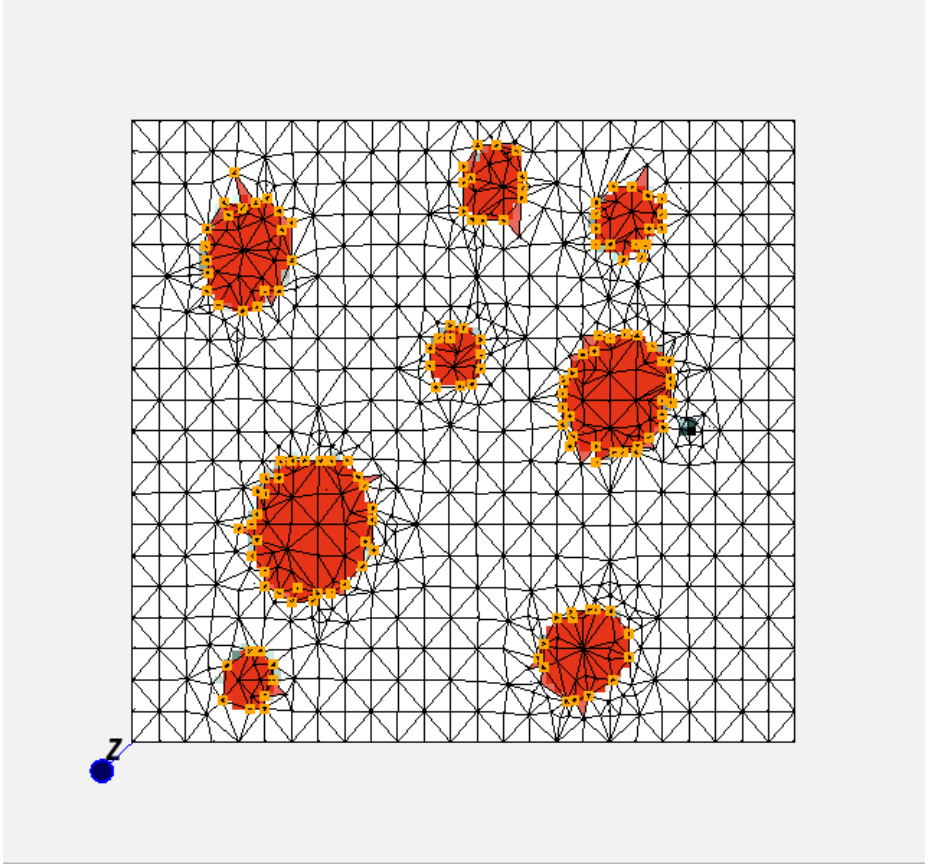

Figure 3.3: Skeleton in OOF3D

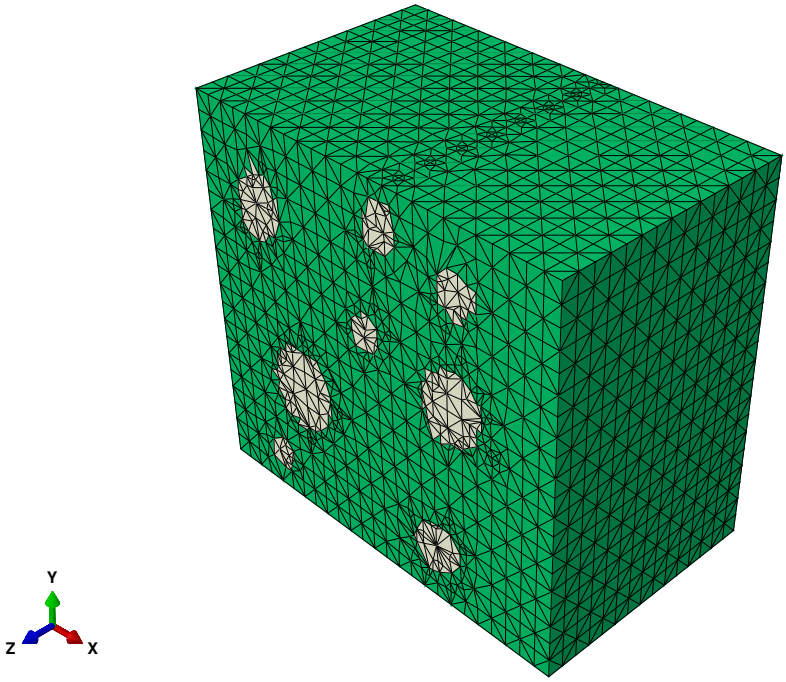

Figure 3.4: FEA model imported from OOF3D

The script is loaded in Abaqus to generate the three dimensional microstructure model. The material properties are not imported and thus have to be assigned in the solver again. FEA was done by applying temperature boundary conditions at the top and bottom surfaces of the microstructure while the other surfaces are insulated.

CHAPTER 4: FINITE ELEMENT ANALYSIS USING MAXWELL'S METHODOLOGY

Maxwell developed his far field methodology to estimate the effective electrical conductivity of isotropic composites. This methodology is analogous to thermal properties and thus is also used in estimating effective thermal conductivity of multi phase composites. Maxwell developed this methodology of estimating electrical conductivity of a cluster of particles embedded in an infinite matrix. The effect of the clusters was considered on the far-field when a uniform electrical field is applied on the whole system. The particle interactions were neglected by adjusting their sizes and distribution in the cluster. These results were only valid for particles with small volume fractions

Maxwell's methodology, which focuses on far-field, can also be applied for prediction of different properties of composite materials. McCartney et al. [6] [26] have shown that this methodology can be used to predict thermal expansion, shear modulus and bulk modulus of multi-phase isotropic composites with homogeneous spherical particles. It is extended to accommodate multi-phase spherical particles with different properties and radii. This technique is reliable to estimate closed form effective properties without the restriction of low volume fractions of the particles.

There are numerous studies conducted to calculate effective thermal conductivity [27]. But most of the studies ignore higher order interactions between the pores and accuracy of the predictions. The periodic problems have accurate analytical and computational techniques [28] [29] [30]. RVE is employed in these methods. There are also numerous techniques available for random arrangement of pores [31].

4.1 Computational technique based on Maxwell's methodology

Olesya Koroteeva et al. [22] have provided an extension of Maxwell's methodology to predict effective thermal conductivity of a porous material in their paper. A semi analytical solution of a problem, where a cluster of non-overlapping spherical particles is embedded into an infinite matrix to which a thermal gradient is applied at infinity, is used. The solutions helps in evaluation of temperatures at points away from the cluster in the matrix.

In a similar problem, an equivalent sphere embedded in the infinite matrix and it has the same thermal properties as that of the composite material. The temperatures are identical at the same finite distance from the equivalent sphere as well as the cluster of non-overlapping spherical particles. Gordeliy el al. [32] provide the semi analytical solution used in the analysis. The steady state heat conduction problem is used here. The temperatures are evaluated at the points distributed on two spheres which are a finite distance away from the cluster and the equivalent sphere. Solid spherical harmonics are adopted to represent the series of temperatures given in the appendix of the paper [1]. For particles of different shapes other than spherical, conventional boundary element method is to be used to solve the problem of infinite space embedded with the cluster of such particles [24]. This computational technique based on Maxwell's methodology can also be applied to elastic multi-phase materials [20] [21].

4.1.1 Cluster of spherical particles in infinite matrix

A finite element model is constructed for the problem with N non-overlapping spherical particles arranged periodically in simple cubic array (SC), body-centered cubic array (BCC) and face centered cubic array (FCC). These spherical pores are constructed in a unit cell. The unit cell with the periodic pore arrangement is embedded in a matrix with unit thermal conductivity k_m. The spherical particles have

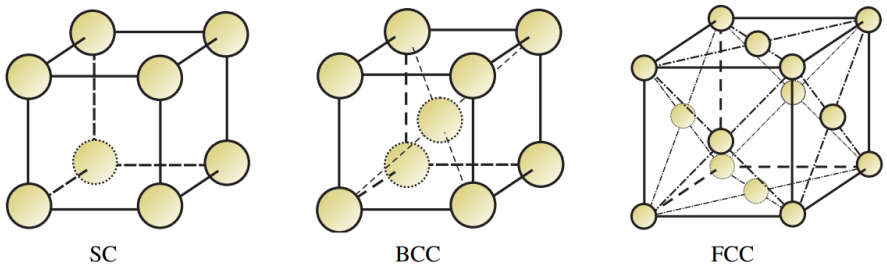

Figure 4.1: Cubical Structures [1]

thermal conductivity k_s which is zero. The radius of the spherical particles are calculated according to the volume fraction or porosity of the composite material by

$$f = N\frac{V_s}{V}. \tag{4.1}$$

Here, N is the number of spherical particles, f is the volume fraction of the composite material, $V_s = \frac{4}{3}\pi r^3$ where r is radius of spherical particle and V is the volume of the unit cube in which the particles are arranged in periodic arrays.

Two cases of each periodic array are constructed for the analysis. The number of spherical particles in the arrays N is varied. The first case has only one array while the second case has eight repetitive arrays arranged. The SC array has 8 spheres and 27 spheres. BCC array has 9 spheres and 35 spheres and FCC array has 14 spheres and 63 spheres.

The volume fraction of single SC array can be given as $f = \frac{4}{3}\pi r^3$. The volume fraction for BCC is given by $\frac{8}{3}\pi r^3$ and its critical volume fraction is given $f_c = \frac{\sqrt{3}}{8}\pi \approx 0.6801748$. While the volume fraction of FCC array is given as $f = \frac{16}{3}\pi r^3$ and its critical volume fraction is $f_c = \frac{\sqrt{2}}{6}\pi \approx 0.7404805$.

4.1.2 Single conducting sphere in infinite matrix

A spherical particle with thermal properties of the composite material is embedded in the cubic matrix for steady state finite element analysis. The effective sphere has thermal conductivity k_s. Continuity conditions of flux and temperature are imposed

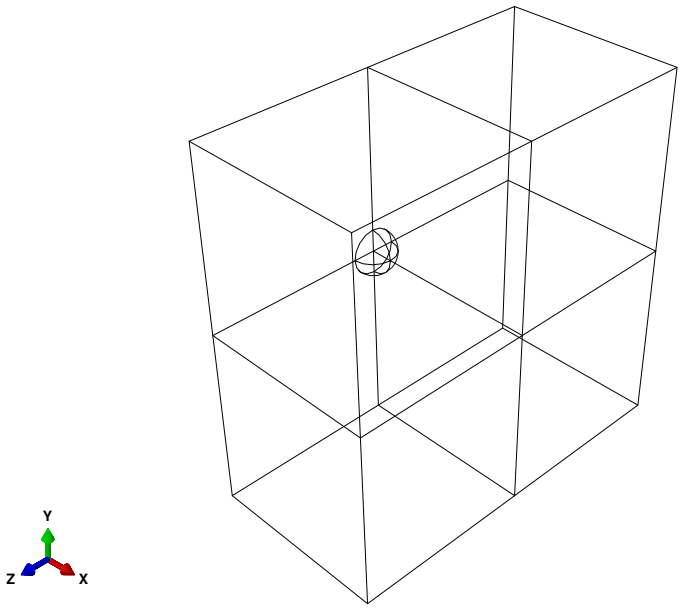

Figure 4.2: Equivalent Spherical inhomogeneity

at the interface of particles and matrix which are:

$$T_s = T_m \tag{4.2}$$

and

$$k_s \frac{T_s}{r} = k_m \frac{T_m}{r}. \tag{4.3}$$

Here, T_m is temperature in the matrix and T_s is temperature in the sphere. The radius of the effective sphere is calculated from

$$f = \sum_{i=1}^{N} R_i^3 / R_{eff}^3 \tag{4.4}$$

where R_{eff} is the radius of effective sphere, R is the radius of spherical pores in the cluster and N is the number of pores [22]. The thermal conductivity of the equivalent spherical particle is the effective thermal conductivity k_{eff}. The effective thermal conductivity for different porosities is calculated in [22]. They are summarized in 4.1-4.3 for cubic, BCC, and FCC arrays respectively.

Table 4.1: Effective thermal conductivity for simple cubic array [22]

Porosity	k_{eff} for 8 sph	k_{eff} for 27 sph
0.1	0.857	0.857
0.2	0.727	0.726
0.3	0.606	0.605
0.4	0.493	0.490
0.5	0.382	0.376
0.5205	0.359	0.351

Table 4.2: Effective thermal conductivity for Body-centered cubic array [22]

Porosity	k_{eff} for 8 sph	k_{eff} for 27 sph
0.1	0.857	0.857
0.2	0.727	0.727
0.3	0.607	0.607
0.4	0.496	0.495
0.5	0.392	0.389
0.6	0.293	0.287
0.6661	0.229	0.219

Table 4.3: Effective thermal conductivity for Face-centered cubic array [22]

Porosity	k_{eff} for 8 sph	k_{eff} for 27 sph
0.1	0.857	0.857
0.2	0.727	0.727
0.3	0.607	0.607
0.4	0.496	0.496
0.5	0.392	0.391
0.6	0.293	0.291
0.7	0.196	0.190
0.7184	0.178	0.171

4.1.3 Single conducting cube in infinite matrix

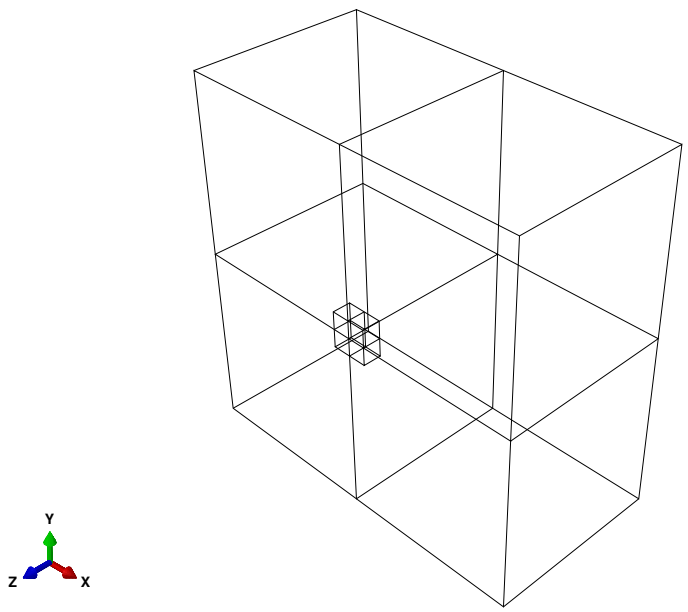

Figure 4.3: Equivalent cubic inhomogeneity

Maxwell's concept has been studied extensively in recent years. Many numerical algorithms are developed in order to obtain accurate solutions for the effective properties of the composite materials. The spherical inhomogeneity considered is found

too restrictive. The use of more general shapes like cube or ellipsoid is suggested by many authors as stated in [23] which was based on the availability of a closed form solution of these shapes. The expression for relating properties of a circular inhomogeneity and a regular shaped inhomogeneity are provided in [23] and [33] . The authors show that if the equivalent homogeneity to be considered have the form of a cube with the same volume as the cluster, the prediction of the effective conductivity of the material converges to the accurate solutions.

A cubic equivalent inhomogeneity is considered in the finite element model. The volume of the cube is equal to the volume of the spherical homogeneity and the volume of the cluster. The inhomgeneity is applied with the same thermal properties as of the spherical inhomogeneity and subsequent results are obtained.

4.1.4 Boundary conditions

The effective thermal conductivity given in the tables are applied to the equivalent inhomogeneity to perform steady state finite element analysis. According to Fourier's law, heat flux is given as $q = -k\nabla T$. The temperature distribution in both the cases is governed by Laplace's equation $\nabla T = 0$. We can write the equation as

$$q_x = -k\frac{\partial T}{\partial x}. \tag{4.5}$$

The temperature normalization or scaling is carried out by setting $\frac{q_0 L}{T_0} = k_0$, we get

$$q_0\bar{q_x} = -\frac{k_0 T_0}{L}\left(\bar{k}\frac{\partial \bar{T}}{\partial \bar{x}}\right). \tag{4.6}$$

With $\bar{x} = \frac{x}{L}$, $\bar{T} = \frac{T}{T_0}$, and $\bar{q}_x = \frac{q_x}{q_0}$, the above equation can be written in non-dimensional form as

$$\bar{q_x} = -\bar{k}\frac{\partial \bar{T}}{\partial \bar{x}}. \tag{4.7}$$

This is the simplification of the temperature gradient to be applied to the cubic matrix. Temperatures 2 and 1 are applied to the top and bottom surfaces respectively, of the matrix cube encompassing the unit cell consisting of the cluster and the equivalent effective sphere. Other sides of the matrix are considered insulated. The models are meshed and finite element analyses are performed.

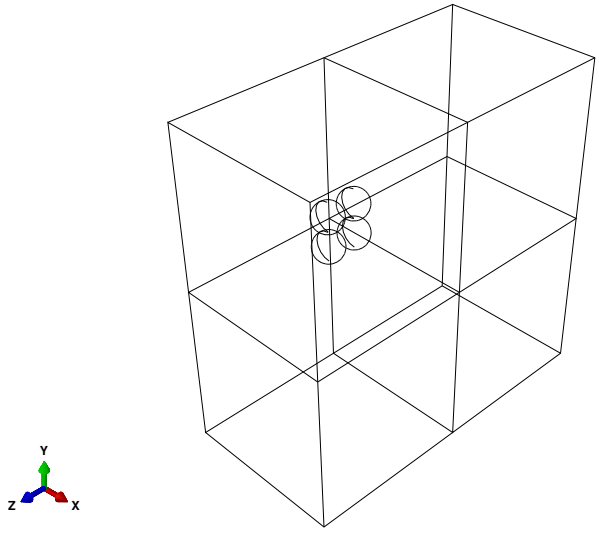

Figure 4.4: Simple cubic array for 8 spherical pores in ABAQUS

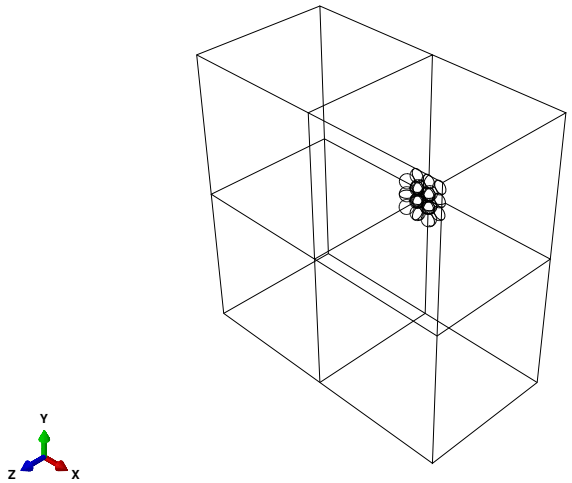

Figure 4.5: Simple cubic array for 27 spherical pores in ABAQUS

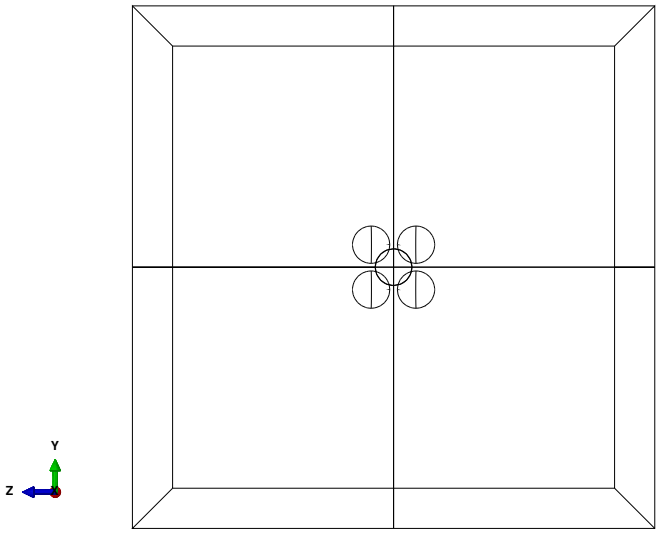

Figure 4.6: Body-centered cubic array for 9 spherical pores in ABAQUS (front view)

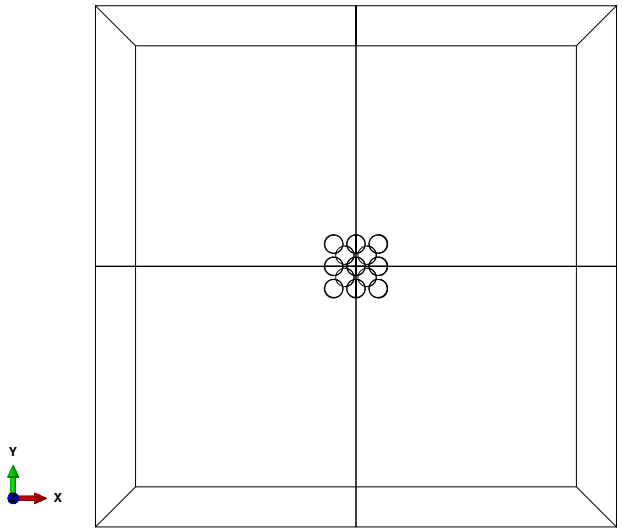

Figure 4.7: Body-centered cubic array for 35 spherical pores in ABAQUS (front view)

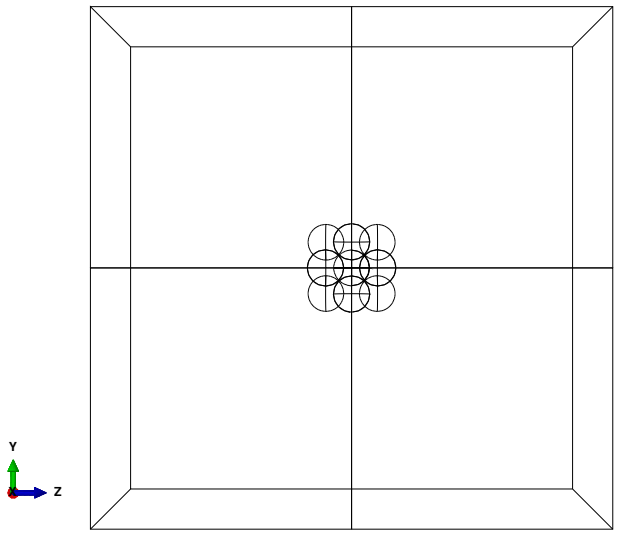

Figure 4.8: Face-centered cubic array for 14 spherical pores in ABAQUS (front view)

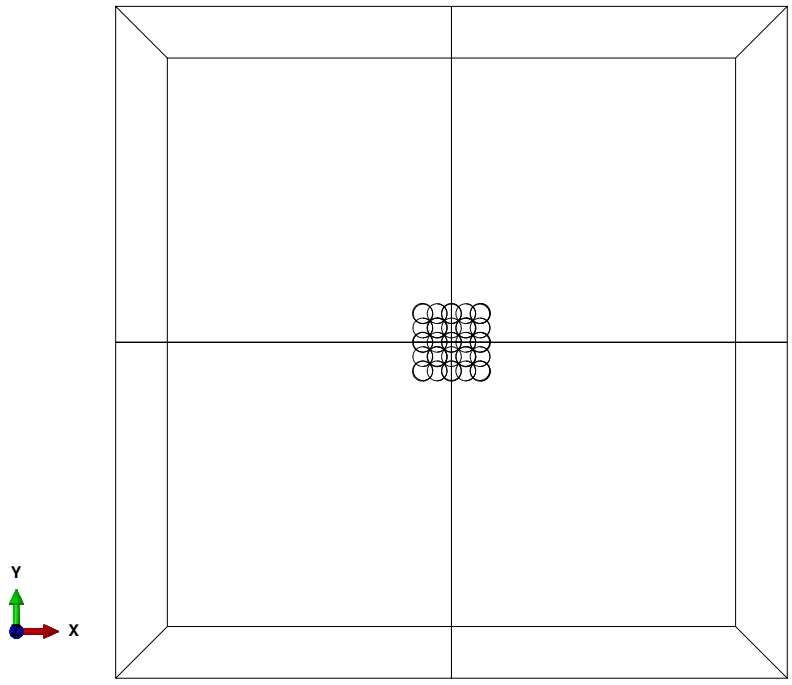

Figure 4.9: Face-centered cubic array for 63 spherical pores in ABAQUS (front view)

CHAPTER 5: EFFECT OF POROSITY ON EFFECTIVE THERMAL CONDUCTIVITY

Effective thermal conductivity changes with change in the porosity of the material. The size and structure of pores also have an impact on the effective thermal conductivity. The relation between the effective thermal conductivity and porosity is established by using three different cases.

5.1 Case 1

In the first case, the pores are through-holes with same diameter. The number of pores is increased from one to eight. Each pore contributes to a porosity of 5% in a unit cube as shown in figure 5.1. Thus, in this case, the porosity varies from 5% to 40%. In figure 5.2, a cube with 40% porosity is shown.

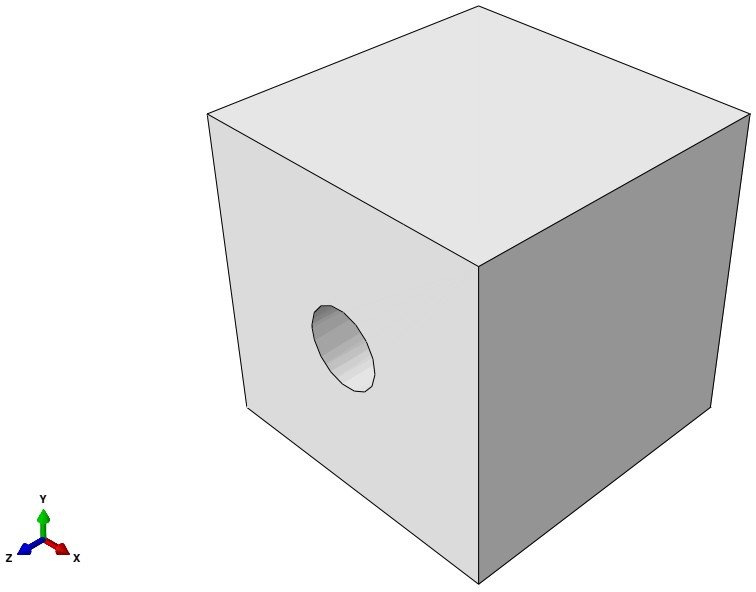

Figure 5.1: Cubic model with single pore with 0.05 porosity

Multiple models of different porosity varying from 0.05 to 0.4 as shown in table 5.1

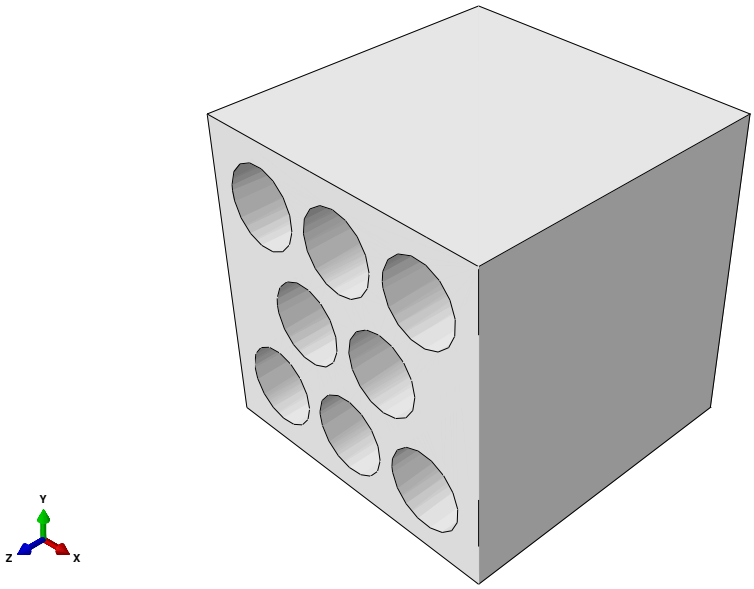

Figure 5.2: Cubic model having 8 pores with 0.4 porosity

are simulated.

Table 5.1: Different cubic models for Case 1

Number of pores	Porosity
1	0.05
2	0.1
3	0.15
4	0.2
5	0.25
6	0.3
7	0.35
8	0.4

5.2 Case 2

In case 2, several porosities are considered just as in case 1. However, for each porosity, multiple pores with different diameters are assumed to be present as shown

in figure 5.3. For porosity of 10%, five cylindrical pores with different dimensions are generated in the model. Three porosities are considered for this case, which are then are divided to obtain five different radii for the pores as shown in the tables 5.2 ,5.3 and 5.4. The pores are again through holes in the cube.

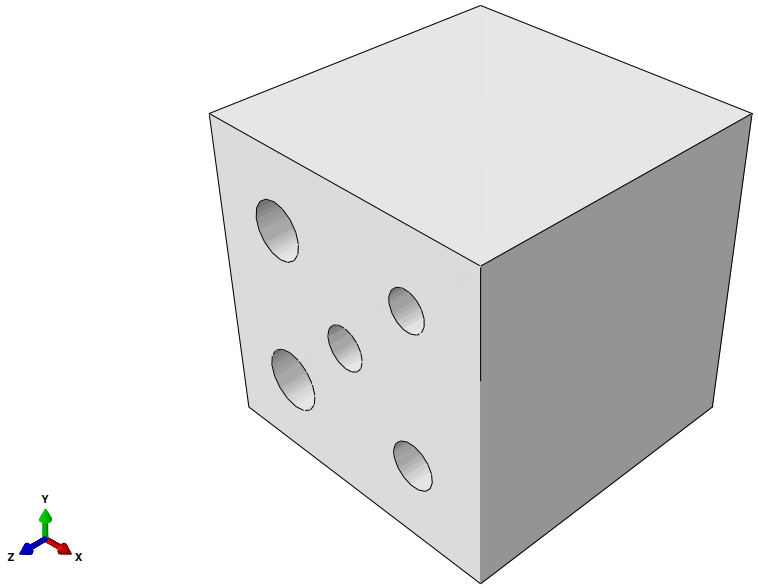

Figure 5.3: Cubic model having different pore geometry with 0.2 porosity

Table 5.2: Different radii of pores for porosity 0.1

Porosity	Radius(m)
0.0125	0.0631
0.015	0.0691
0.0175	0.0746
0.025	0.0892
0.03	0.0977

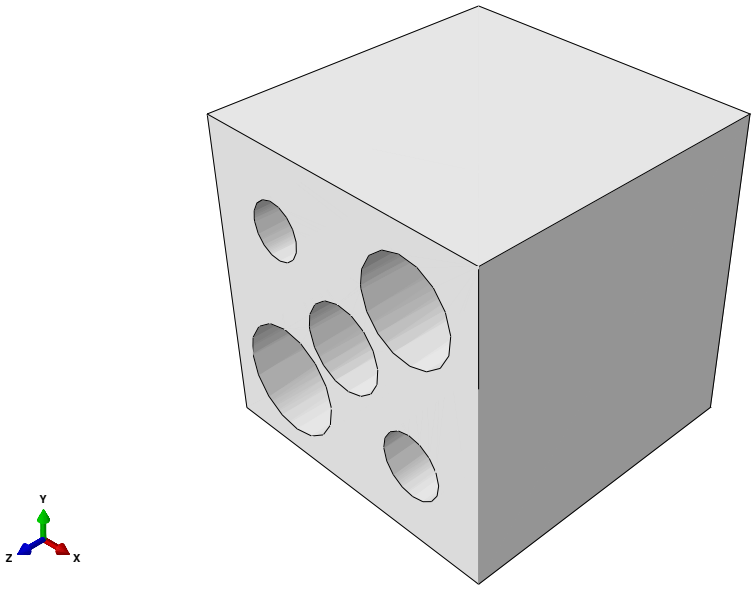

Figure 5.4: Cubic model having different pore geometry with 0.3 porosity

Table 5.3: Different radii of pores for porosity 0.2

Porosity	Radius(m)
0.015	0.00691
0.02	0.0798
0.035	0.1056
0.05	0.1262
0.08	0.1596

Table 5.4: Different radii of pores for porosity 0.3

Porosity	Radius(m)
0.025	0.0892
0.035	0.1056
0.06	0.1392
0.08	0.1596
0.1	0.1794

5.3 Case 3

Third case has spherical pores embedded in the cubic structure as shown in figure 5.5. These pores contribute to 2.5% porosity each. The pores are arranged randomly in the cube. Similar to the first case, the number of pores are increased to increase the porosity. The pores are arranged randomly in the cube. Models with with two, four and six pores are generated with porosity 0.5, 0.1 and 0.15 respectively.

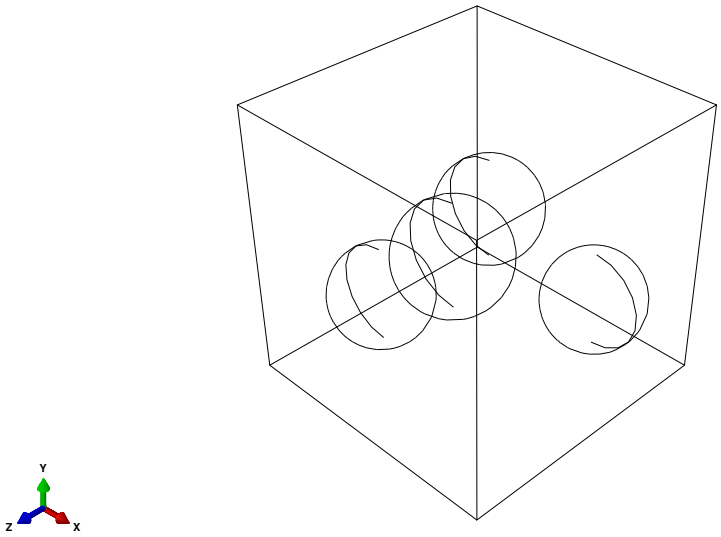

Figure 5.5: Wire frame view of cubic model embedded with four spherical pores

5.4 Boundary conditions

In all the cases, the thermal conductivity of the model is $1W/m-K$. The top and bottom surface of the cube are applied temperature boundary condition of 200 C and 100 C respectively. The other sides of the cube are taken to be insulated. The same material properties and boundary conditions are used in all three cases. Steady-state thermal analysis is carried out to obtain average heat flux values on the top surface of the cube.

CHAPTER 6: RESULTS

6.1 Imaged-based FEA results

Steady state thermal analysis is carried out on the model generated by OOF3D. The top and bottom boundaries are prescribed temperatures of 200°C and 100°C, respectively. The other four faces of the model are considered adiabatic. Figure 6.1 and 6.2 shows the heat flux distribution and the nodal temperatures changes due to the pores.

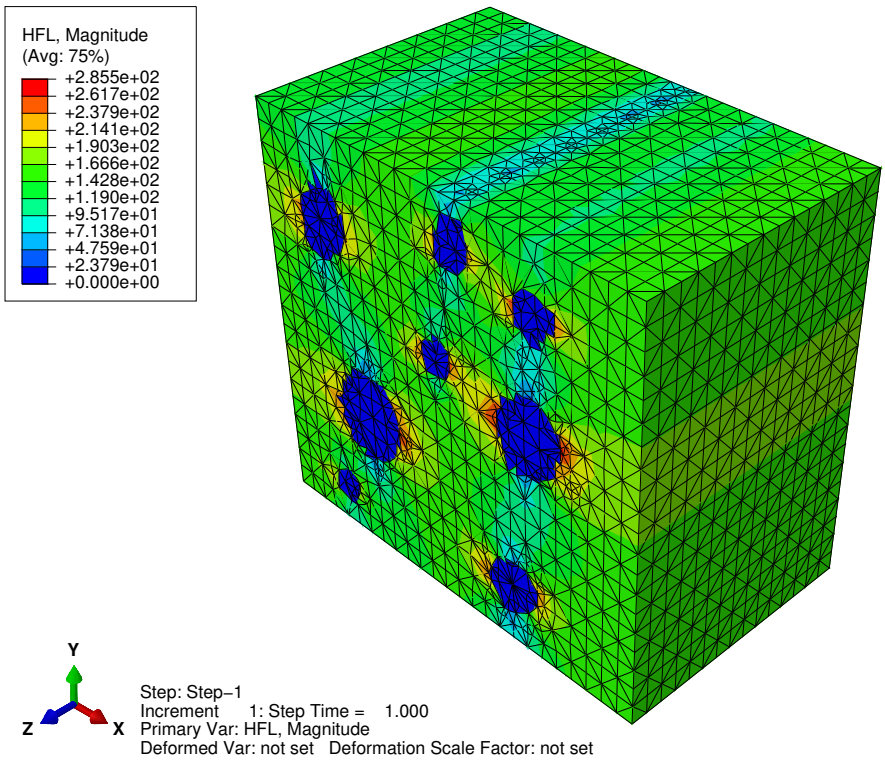

Figure 6.1: Heat flux magnitude in the cubic model with single pore with 0.05 porosity.

The effective thermal conductivity can be calculated by using the average heat flux

on the top surface of the model [3] given by

$$k_{eff} = \frac{\sum q/W}{\Delta T/L}. \tag{6.1}$$

Here, q is the vertical heat flux on the top surface. We get k_{eff} as 92.01615 $W/m°C$. This is just an analytical value for a trial micro-structure for which ceramic thermal conductivity was considered as 120 $W/m°C$. The effective thermal conductivity is lower than the thermal conductivity of a solid material due to the effects of pores.

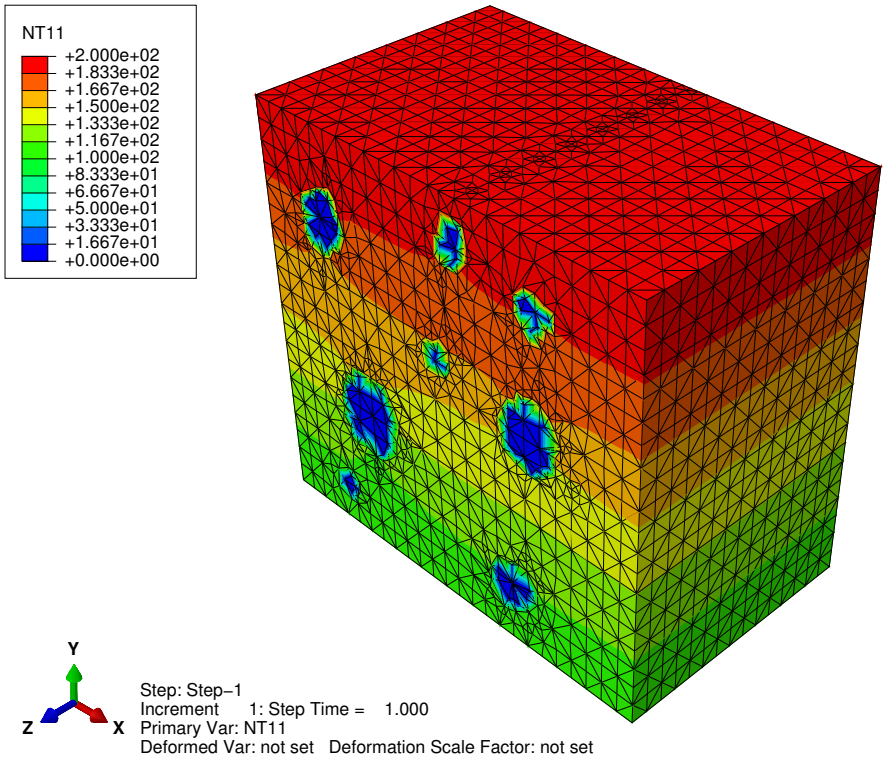

Figure 6.2: Nodal Temperature for the model

6.2 Results for Maxwell's methodology

Maxwell's methodology states that the temperature at far-field is equal for both the cluster and the equivalent inhomogeneity. Steady state thermal analysis is carried out on all three types of arrays and their corresponding equivalent spherical and cubical inhomogeneity. Temperature profile is obtained for all the cases with the pathway going from the center of the cube to its top surface. The porosity is increased for each case and the k_{eff} property is applied to the equivalent inhomogeneity using the values from Tables 4.1 to 4.3. Temperature profiles are compared for all the cases in the plots for the given porosity in the sections further for different arrangement of pores in the cluster.

6.2.1 Simple Cubic arrangement of pores

Heat flux and nodal temperatures are calculated by steady state thermal analysis of the matrix containing the cluster and equivalent inhomogeneity. 50 data points were used to plot the temperature from the center of the matrix to the top surface. The plots from Fig. 6.3 to 6.14 show the comparison of temperature distribution for simple cubic array of particles and the spherical and cubical inhomogeneity. The k_{eff} values for different porosity and number of spherical particles are shown in Table 4.1. The temperatures are similar for porosity lower than 0.3. There is a deviation for clusters with porosity greater than 0.3 and all the temperature plots converge after a specific distance from the array and the equivalent inhomgeneity. The drop in the temperature in the plots denotes the presence of pores in the pathway.

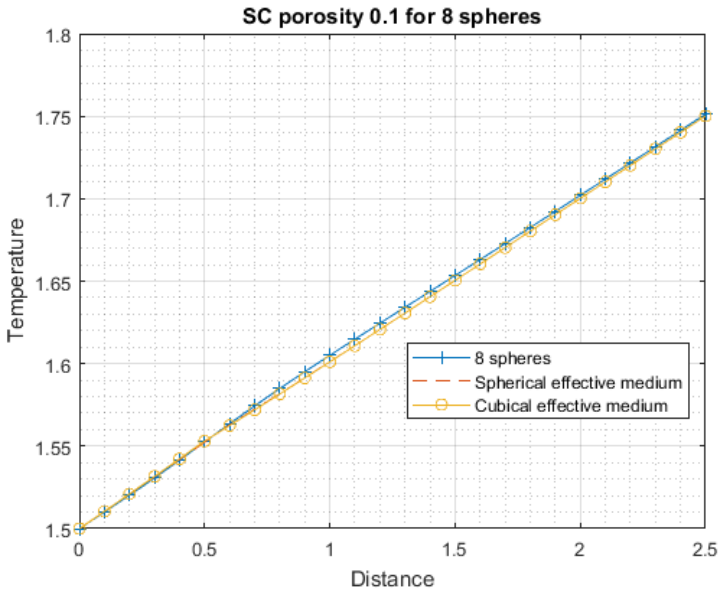

Figure 6.3: Plot of SC cluster with porosity 0.1 for 8 pores vs spherical effective medium vs cubic effective medium

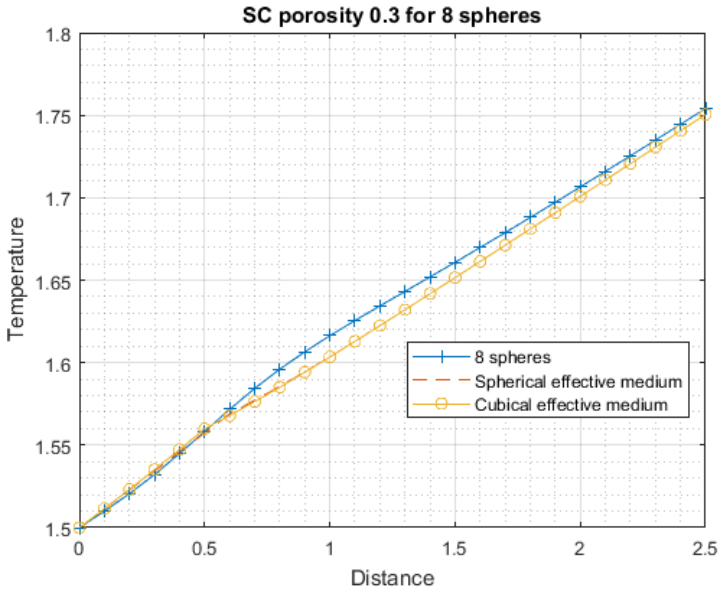

Figure 6.5: Plot of SC cluster with porosity 0.3 for 8 pores vs spherical effective medium vs cubic effective medium

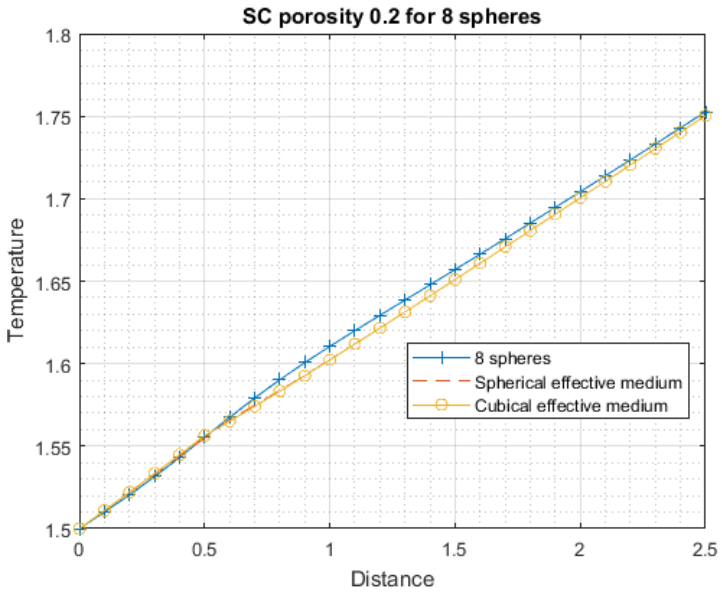

Figure 6.4: Plot of SC cluster with porosity 0.2 for 8 pores vs spherical effective medium vs cubic effective medium

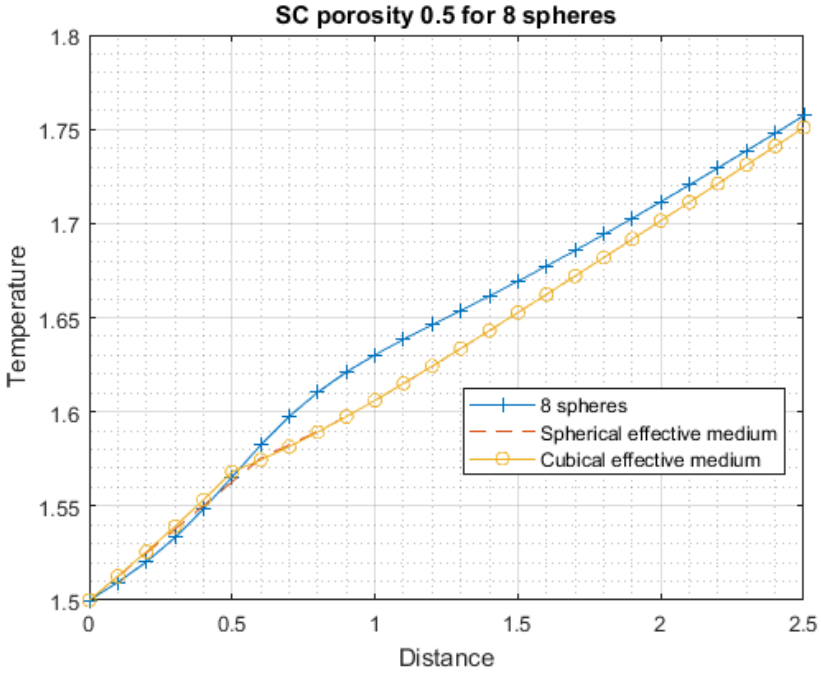

Figure 6.7: Plot of SC cluster with porosity 0.5 for 8 pores vs spherical effective medium vs cubic effective medium

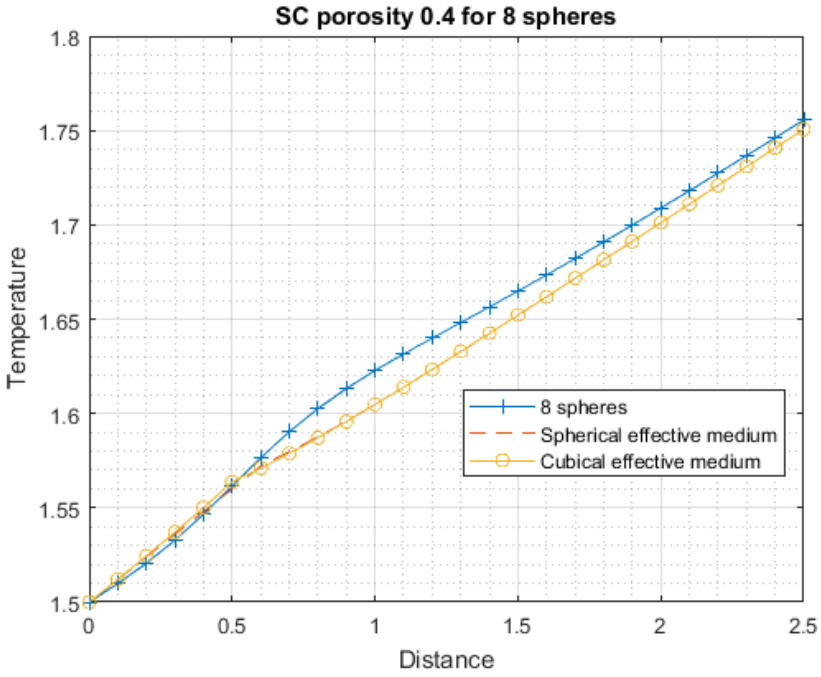

Figure 6.6: Plot of SC cluster with porosity 0.4 for 8 pores vs spherical effective medium vs cubic effective medium

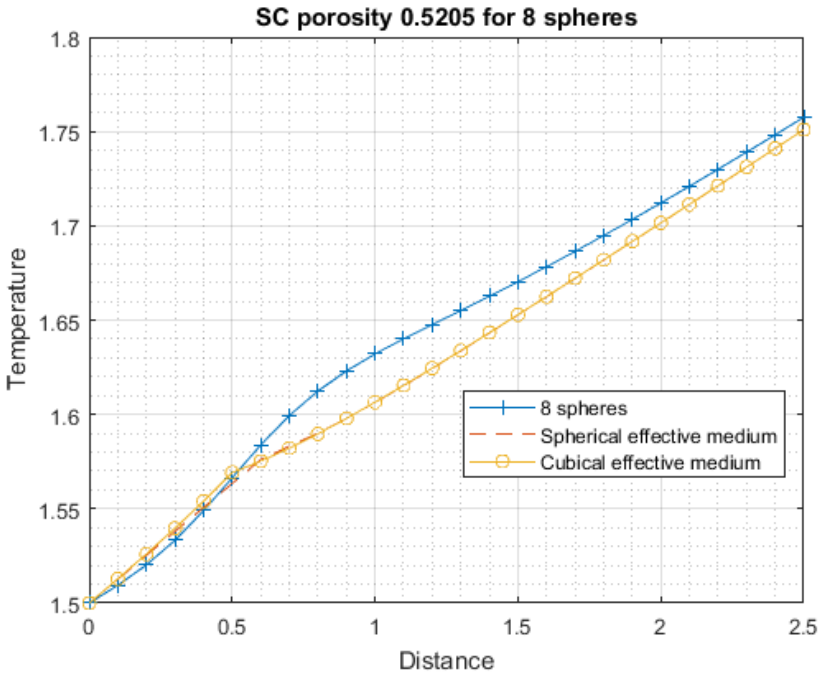

Figure 6.8: Plot of SC cluster with porosity 0.5205 for 8 pores vs spherical effective medium vs cubic effective medium

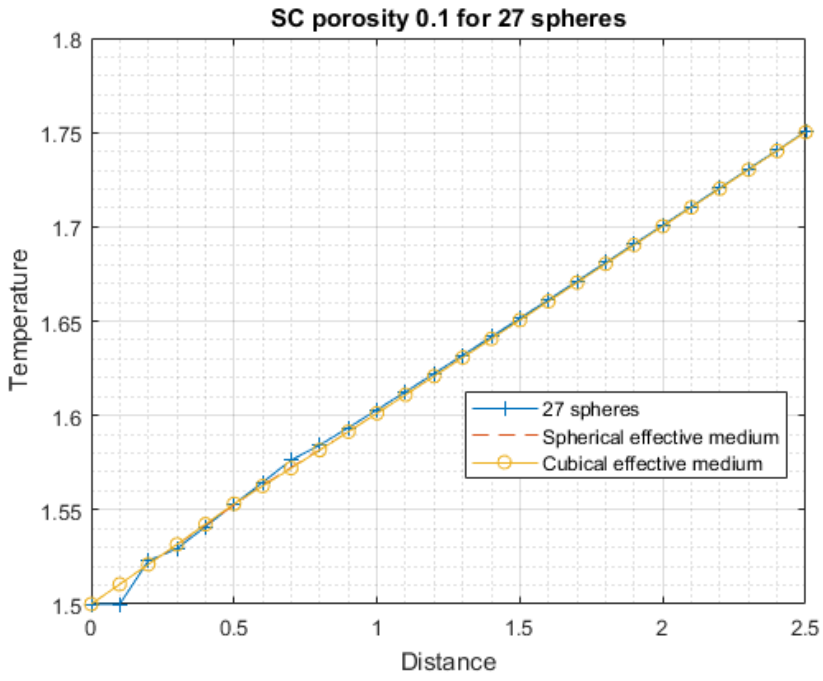

Figure 6.9: Plot of SC cluster with porosity 0.1 for 27 pores vs spherical effective medium vs cubic effective medium

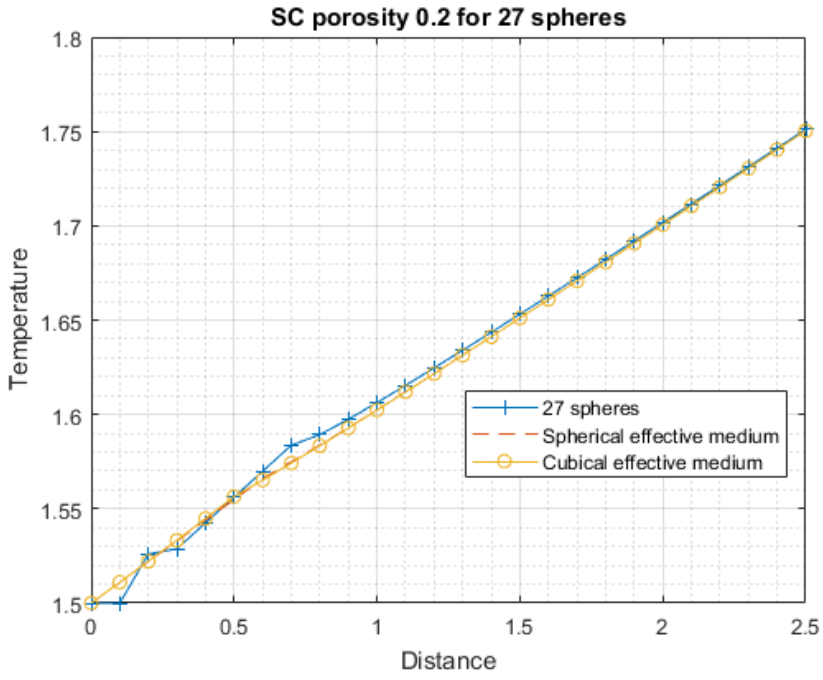

Figure 6.10: Plot of SC cluster with porosity 0.2 for 27 pores vs spherical effective medium vs cubic effective medium

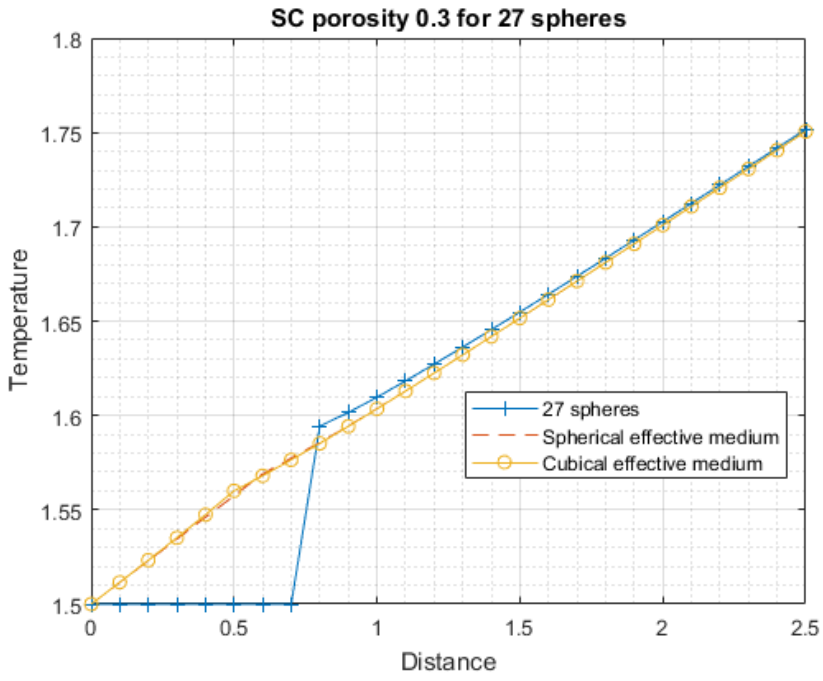

Figure 6.11: Plot of SC cluster with porosity 0.3 for 27 pores vs spherical effective medium vs cubic effective medium

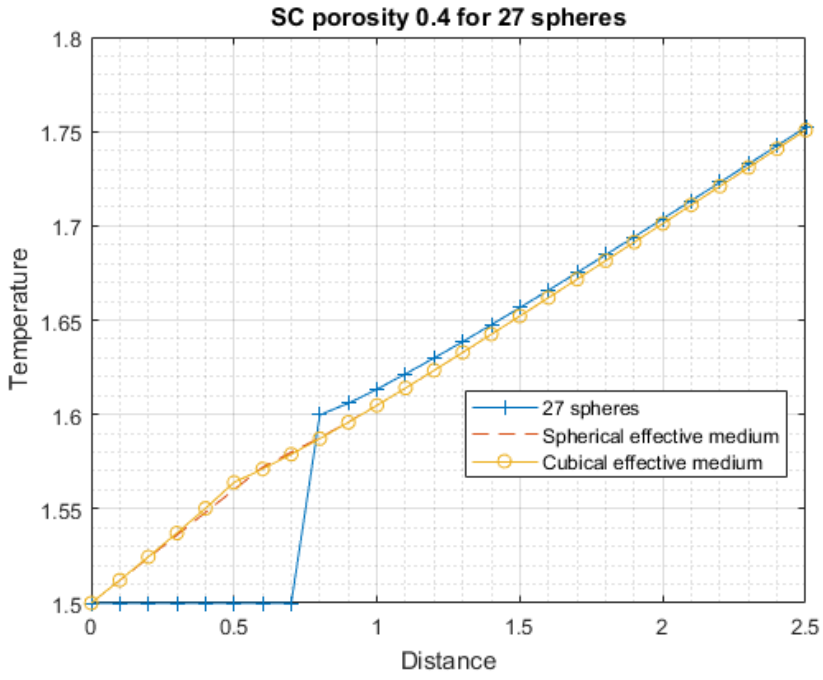

Figure 6.12: Plot of SC cluster with porosity 0.4 for 27 pores vs spherical effective medium vs cubic effective medium

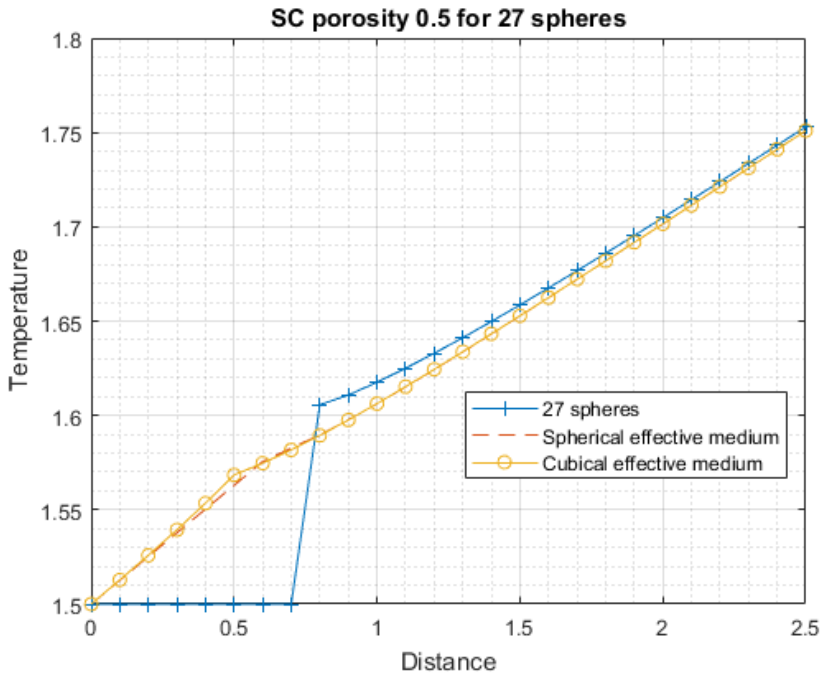

Figure 6.13: Plot of SC cluster with porosity 0.5 for 27 pores vs spherical effective medium vs cubic effective medium

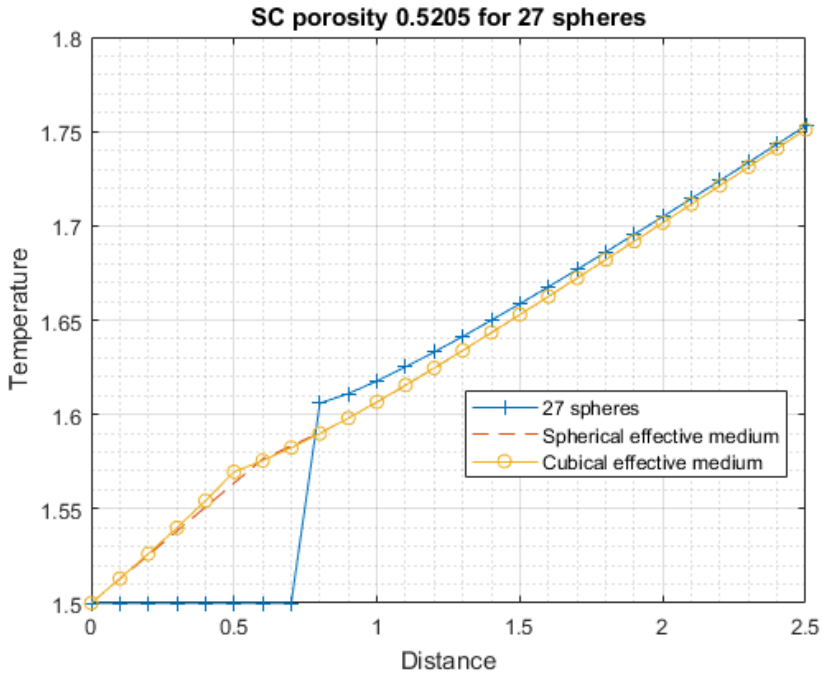

Figure 6.14: Plot of SC cluster with porosity 0.5205 for 27 pores vs spherical effective medium vs cubic effective medium

6.2.2 Body Centered Cubic arrangement of pores

Similar to the SC arrangement, the pores are arranged in BCC and the heat flux and nodal temperatures are calculated. The k_{eff} values for different porosity and number of spherical particles are shown in Table 4.2. The plots from Fig. 6.15 to 6.28 shows the comparison of the temperature distribution between body-centered cubic array of pores and the spherical and cubical inhomogeneity by increasing the porosity. The plots are presented for both 9 and 35 number of pores in the cubic structure. The temperature profile deviates from the center of the cube for all three cases and converges at the far field. The deviation increases with increase in porosity. The sudden drop in the temperature profile denotes the presence of pores in the pathway.

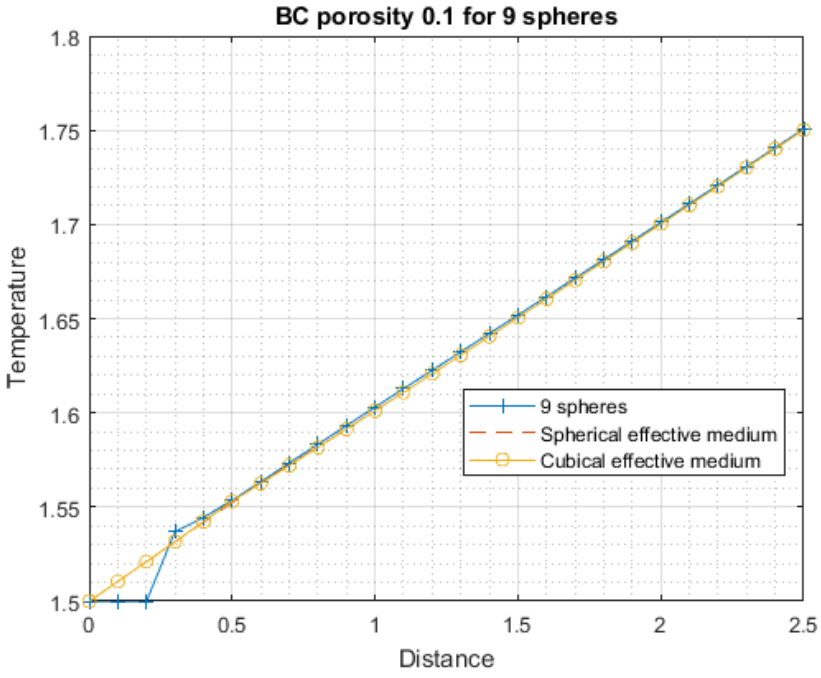

Figure 6.15: Plot of BCC cluster with porosity 0.1 for 9 pores vs spherical effective medium vs cubic effective medium

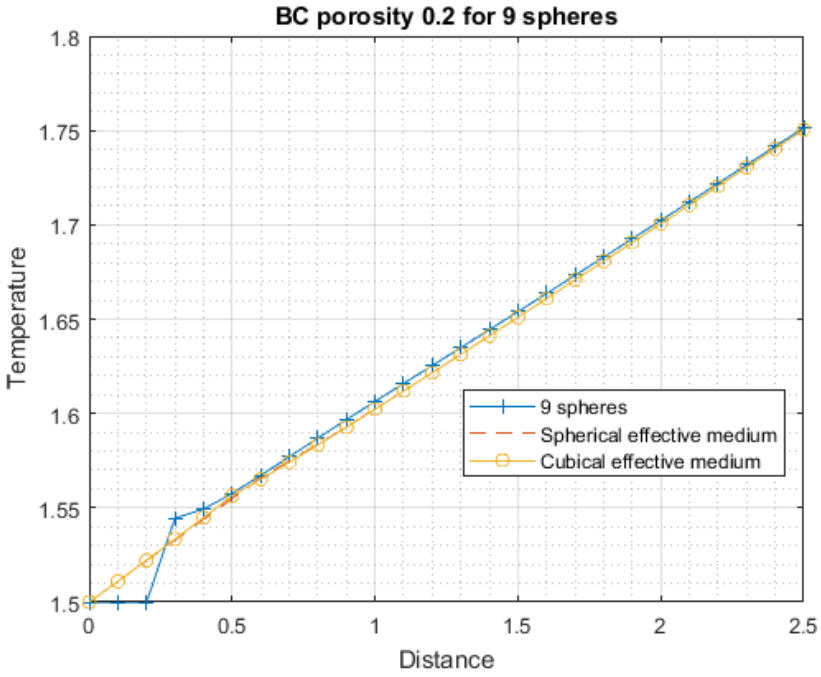

Figure 6.16: Plot of BCC cluster with porosity 0.2 for 9 pores vs spherical effective medium vs cubic effective medium

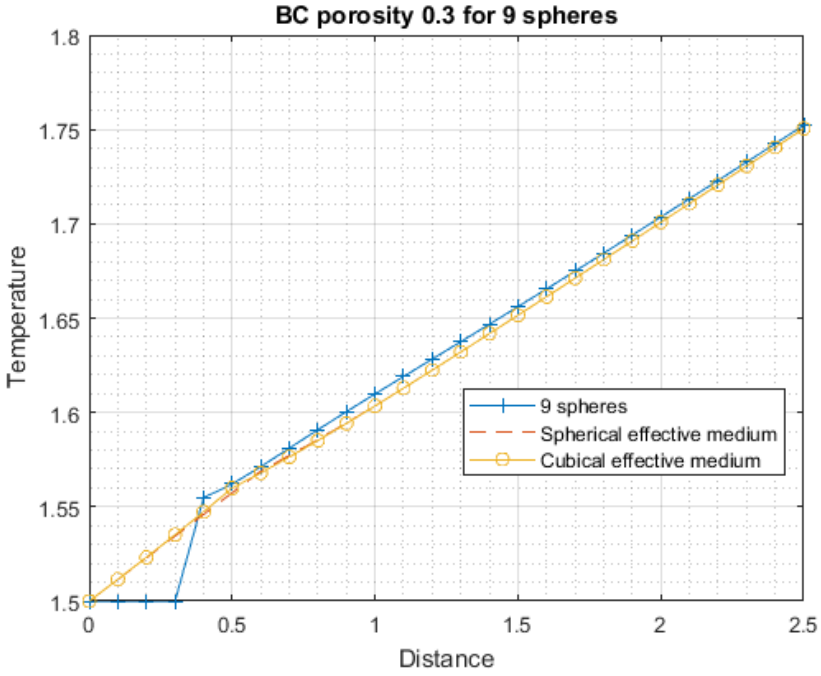

Figure 6.17: Plot of BCC cluster with porosity 0.3 for 9 pores vs spherical effective medium vs cubic effective medium

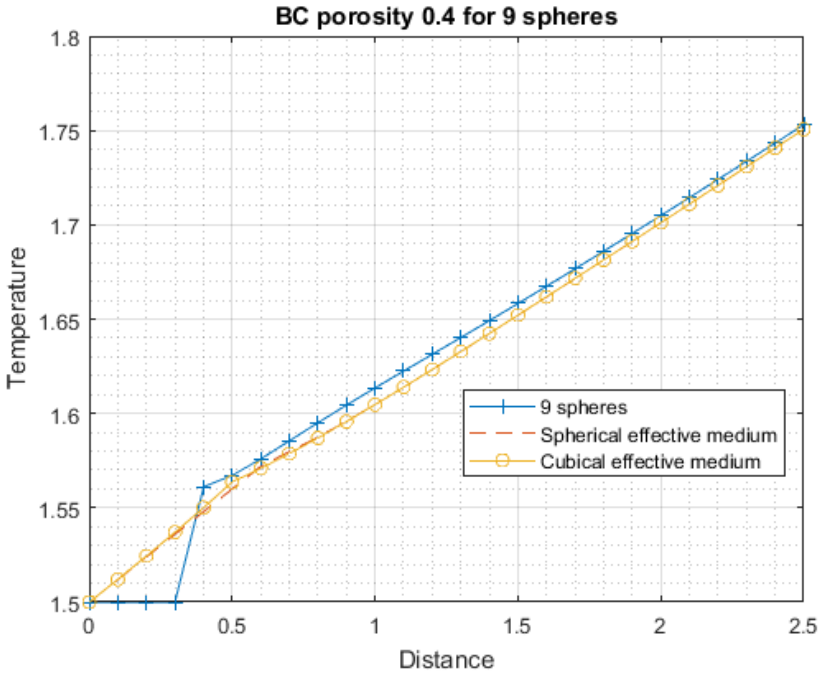

Figure 6.18: Plot of BCC cluster with porosity 0.4 for 9 pores vs spherical effective medium vs cubic effective medium

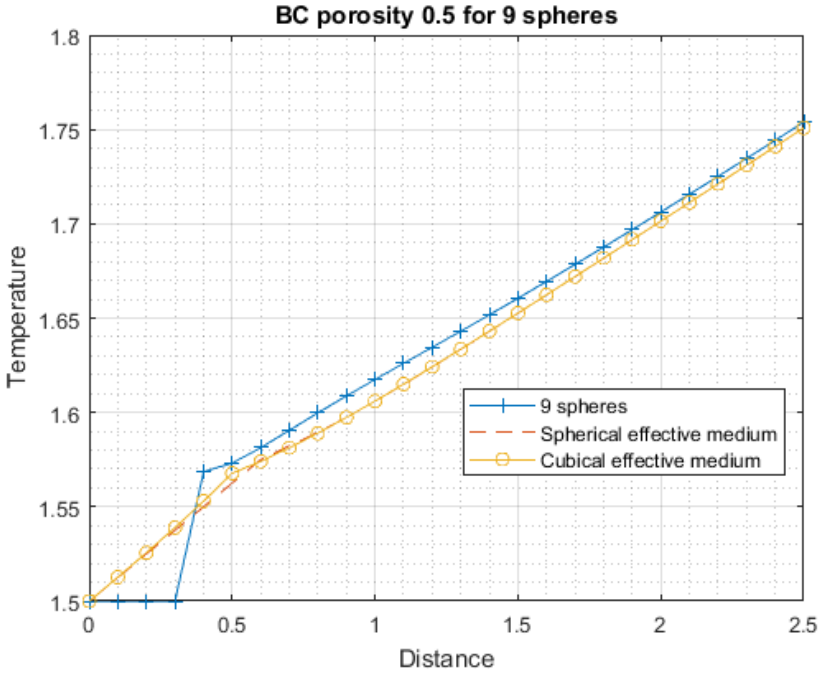

Figure 6.19: Plot of BCC cluster with porosity 0.5 for 9 pores vs spherical effective medium vs cubic effective medium

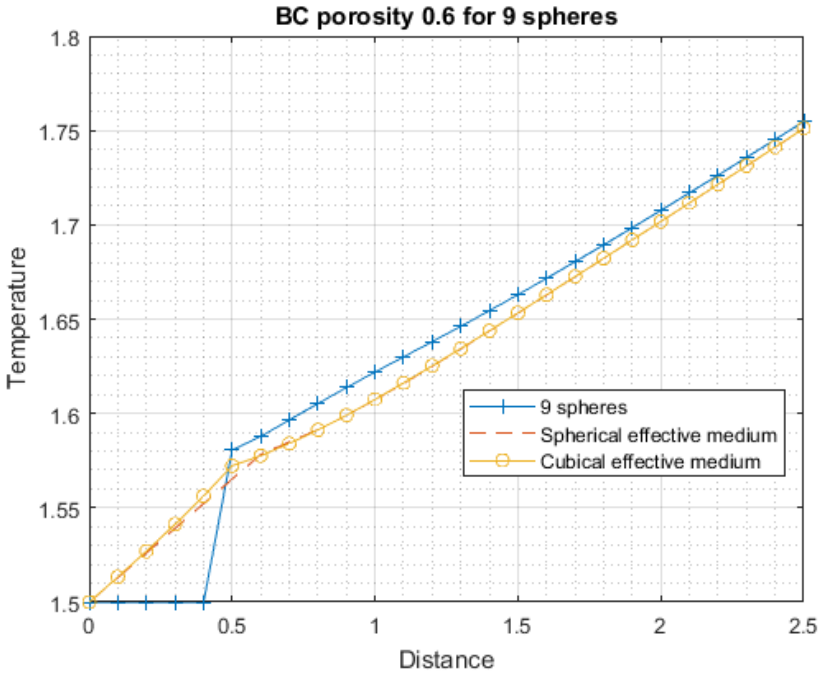

Figure 6.20: Plot of BCC cluster with porosity 0.6 for 9 pores vs spherical effective medium vs cubic effective medium

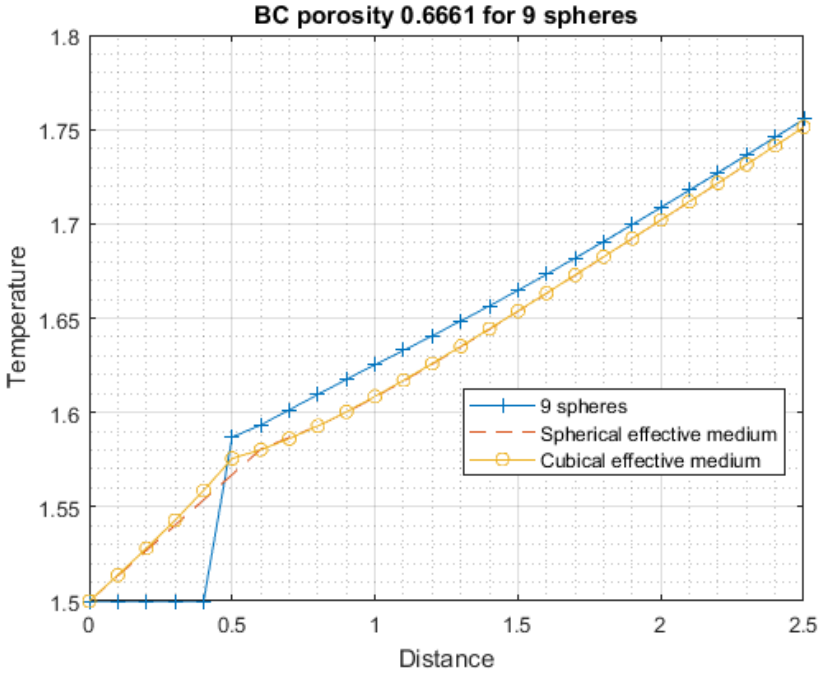

Figure 6.21: Plot of BCC cluster with porosity 0.6661 for 9 pores vs spherical effective medium vs cubic effective medium

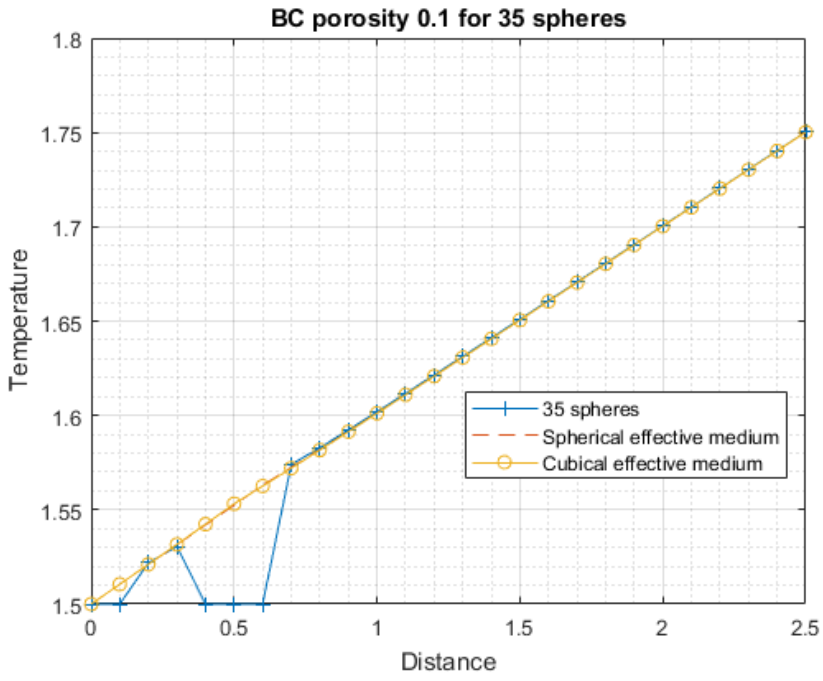

Figure 6.22: Plot of BCC cluster with porosity 0.1 for 35 pores vs spherical effective medium vs cubic effective medium

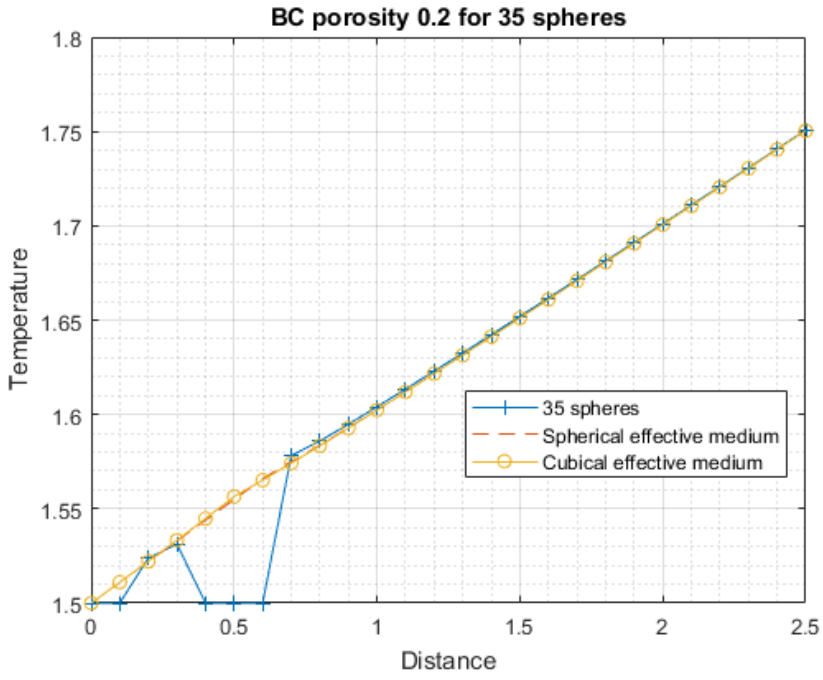

Figure 6.23: Plot of BCC cluster with porosity 0.2 for 35 pores vs spherical effective medium vs cubic effective medium

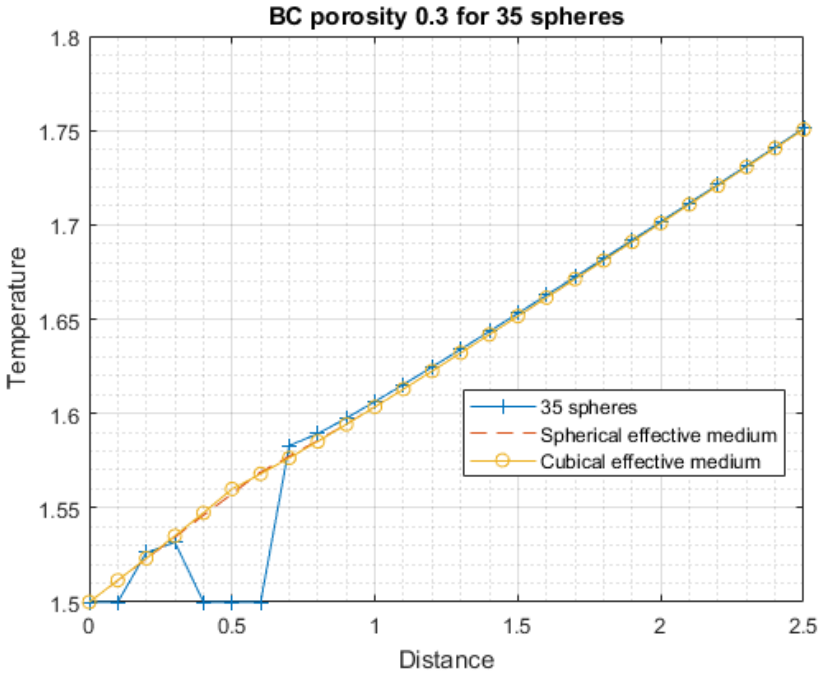

Figure 6.24: Plot of BCC cluster with porosity 0.3 for 35 pores vs spherical effective medium vs cubic effective medium

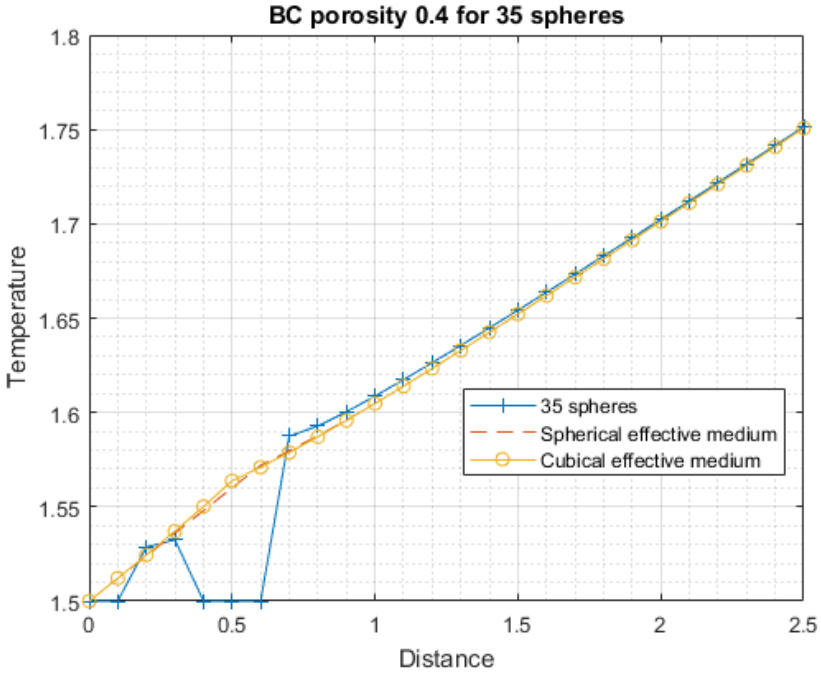

Figure 6.25: Plot of BCC cluster with porosity 0.4 for 35 pores vs spherical effective medium vs cubic effective medium

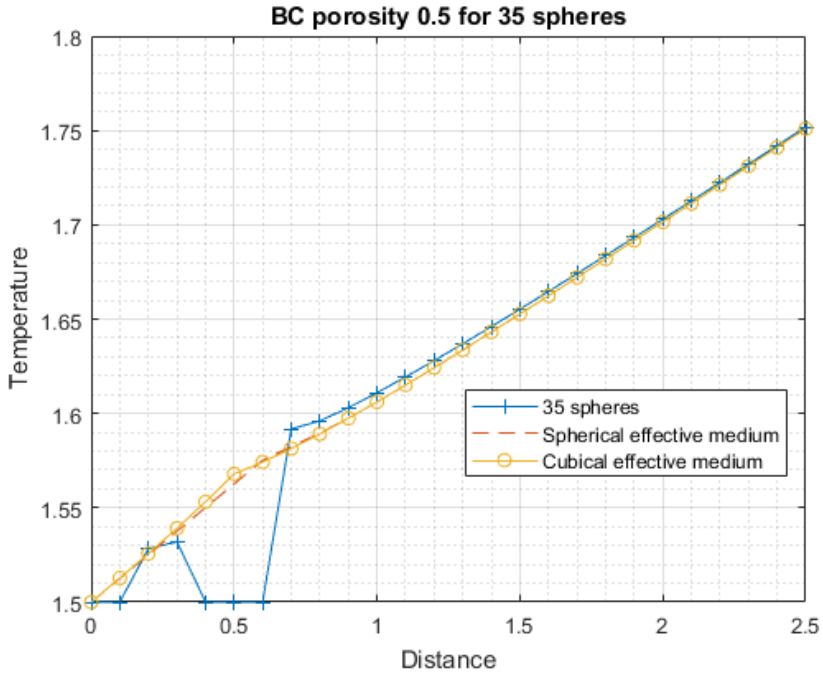

Figure 6.26: Plot of BCC cluster with porosity 0.5 for 35 pores vs spherical effective medium vs cubic effective medium

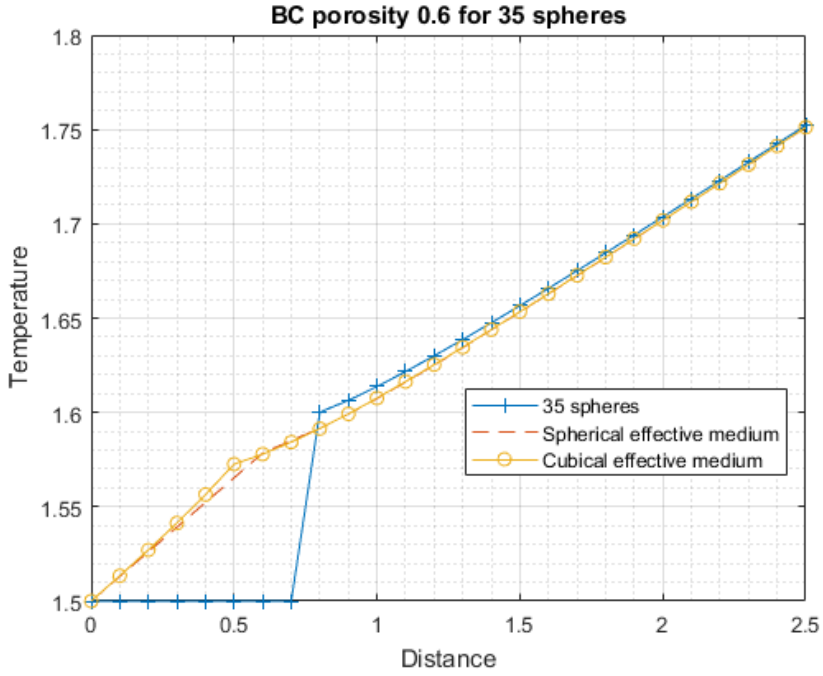

Figure 6.27: Plot of BCC cluster with porosity 0.6 for 35 pores vs spherical effective medium vs cubic effective medium

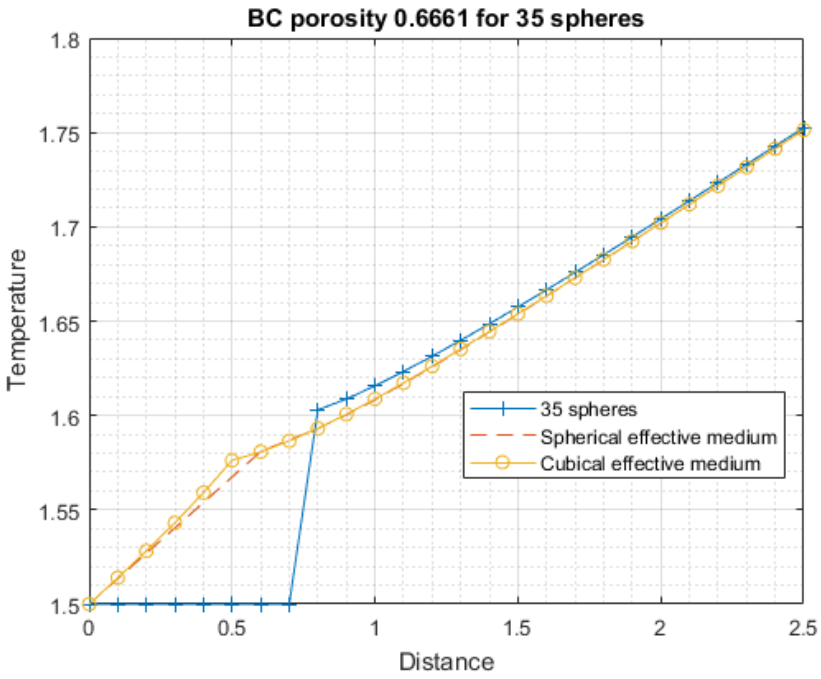

Figure 6.28: Plot of BCC cluster with porosity 0.6661 for 35 pores vs spherical effective medium vs cubic effective medium

6.2.3 Face Centered Cubic arrangement of pores

The steady state thermal analysis results for heat flux and temperature for pores arranged in face-centered cubic structure is presented below from Fig. 6.29 to 6.44. The k_{eff} values for different porosity and number of spherical particles are shown in Table 4.3. Similar to the above two cases, the temperature deviation is seen in the profile which increases with increase in porosity. The plots show the comparison of the three cases wherein the number of pores are 14 and 63 with varying porosity for both the cases. The plots show similar drop of temperature at the presence of pores in the pathways. This drop indicates the adiabatic boundary condition in the pores as no radiation is considered.

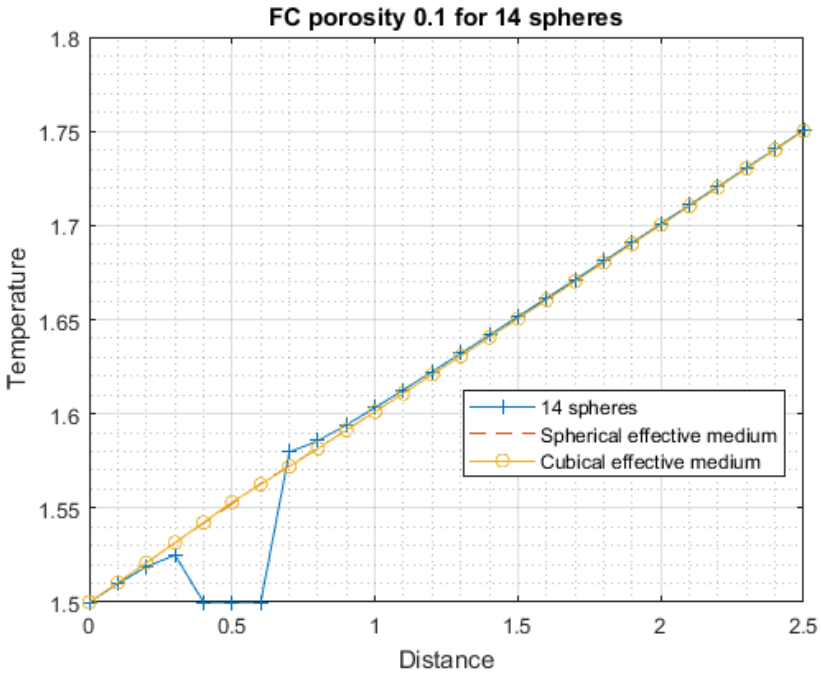

Figure 6.29: Plot of FCC cluster with porosity 0.1 for 14 pores vs spherical effective medium vs cubic effective medium

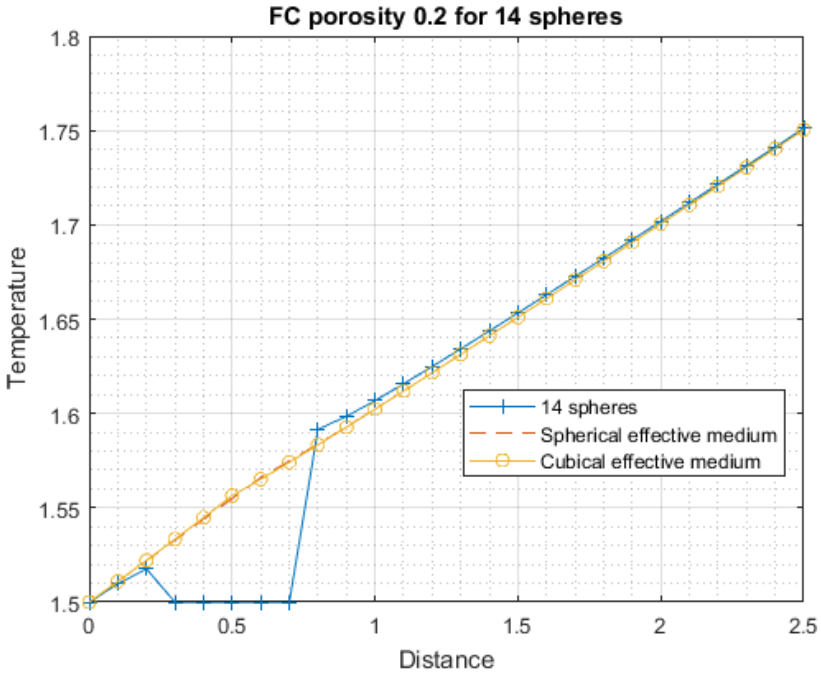

Figure 6.30: Plot of FCC cluster with porosity 0.2 for 14 pores vs spherical effective medium vs cubic effective medium

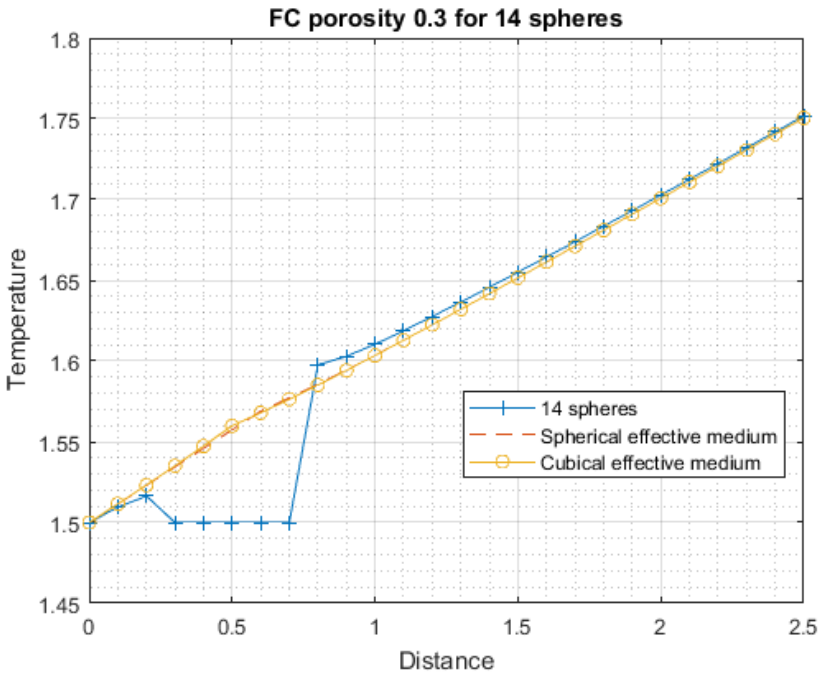

Figure 6.31: Plot of FCC cluster with porosity 0.3 for 14 pores vs spherical effective medium vs cubic effective medium

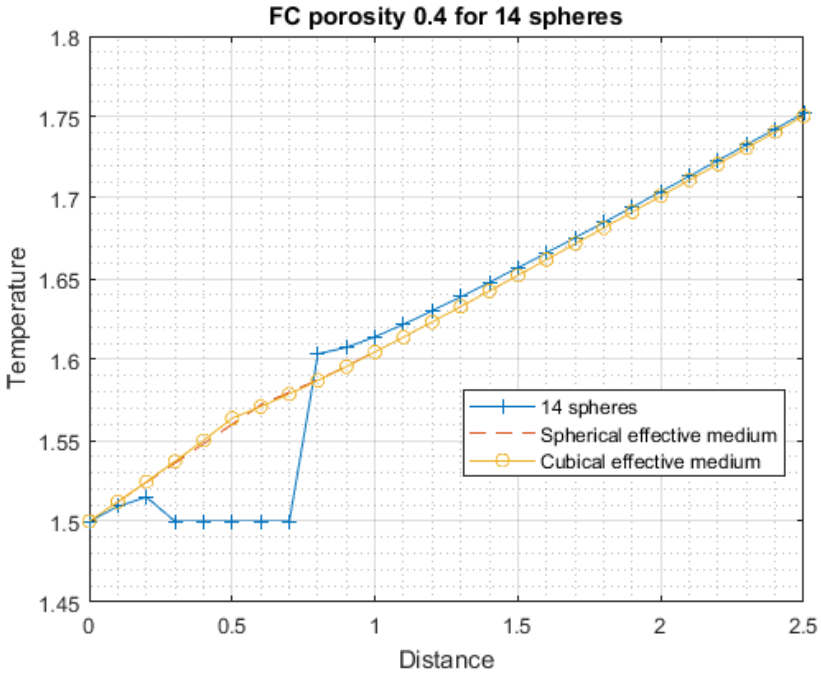

Figure 6.32: Plot of FCC cluster with porosity 0.4 for 14 pores vs spherical effective medium vs cubic effective medium

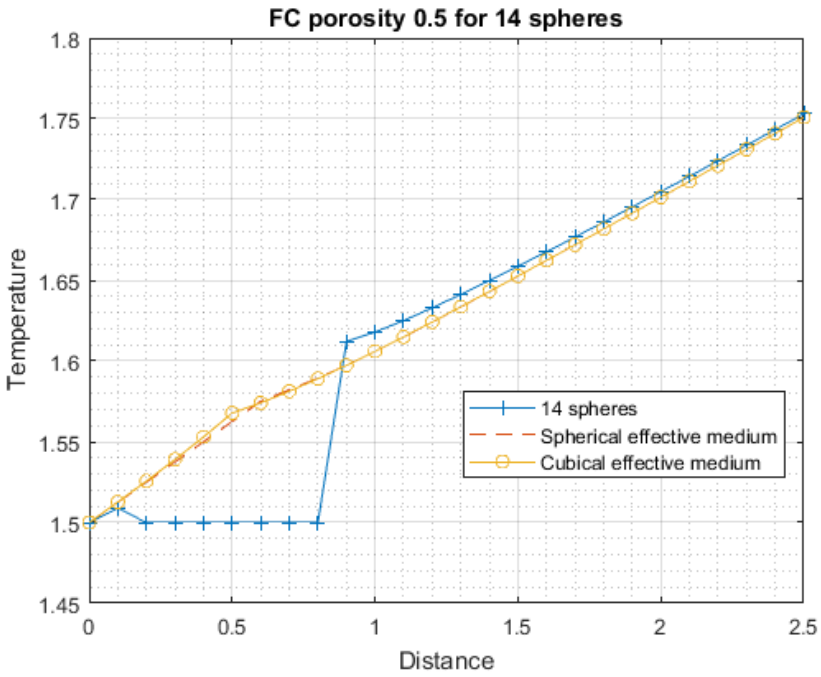

Figure 6.33: Plot of FCC cluster with porosity 0.5 for 14 pores vs spherical effective medium vs cubic effective medium

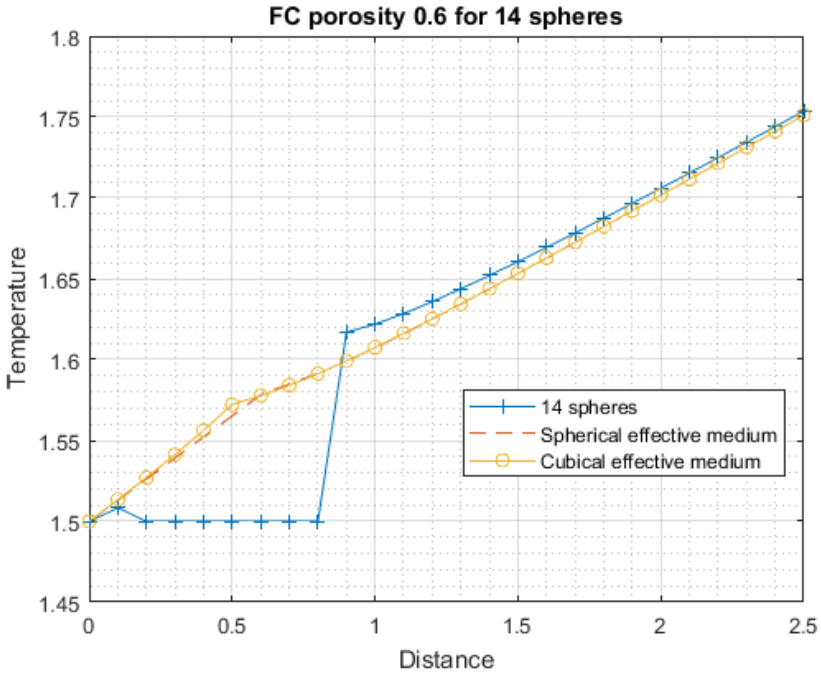

Figure 6.34: Plot of FCC cluster with porosity 0.6 for 14 pores vs spherical effective medium vs cubic effective medium

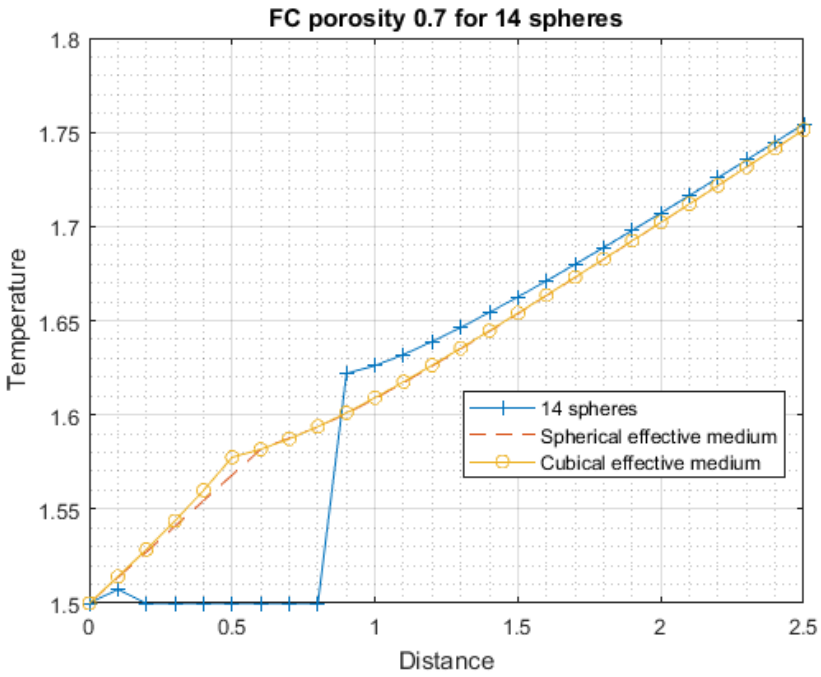

Figure 6.35: Plot of FCC cluster with porosity 0.7 for 14 pores vs spherical effective medium vs cubic effective medium

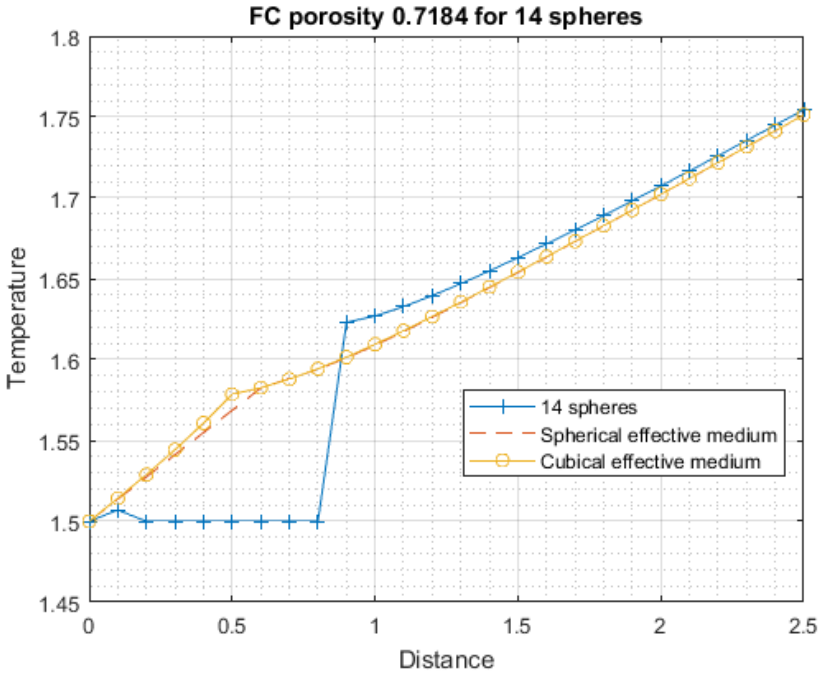

Figure 6.36: Plot of FCC cluster with porosity 0.7184 for 14 pores vs spherical effective medium vs cubic effective medium

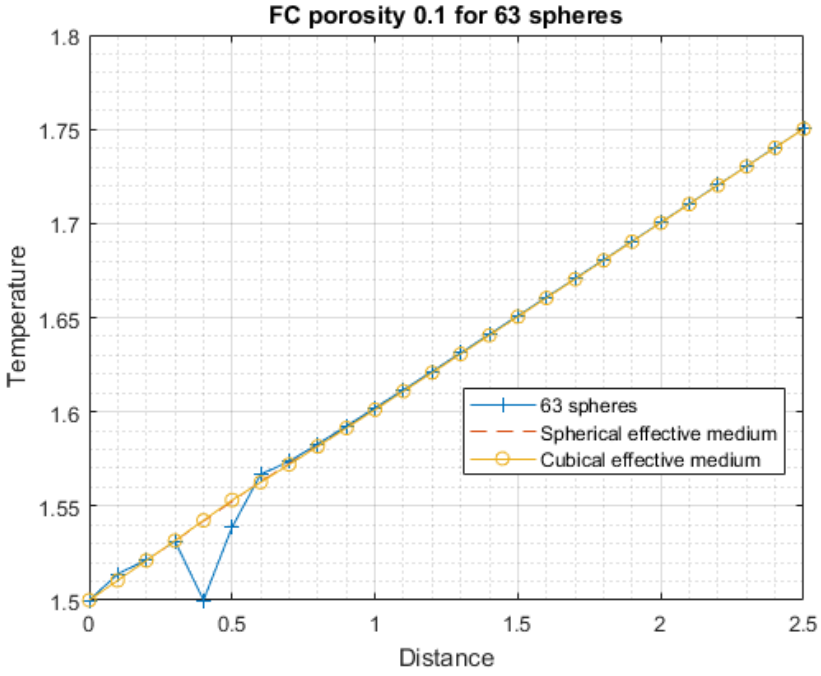

Figure 6.37: Plot of FCC cluster with porosity 0.1 for 63 pores vs spherical effective medium vs cubic effective medium

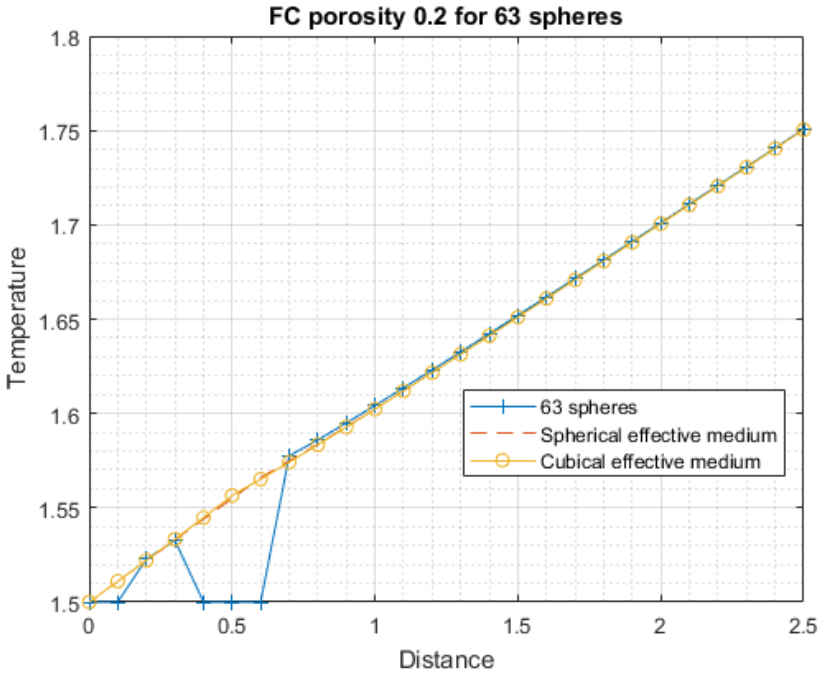

Figure 6.38: Plot of FCC cluster with porosity 0.2 for 63 pores vs spherical effective medium vs cubic effective medium

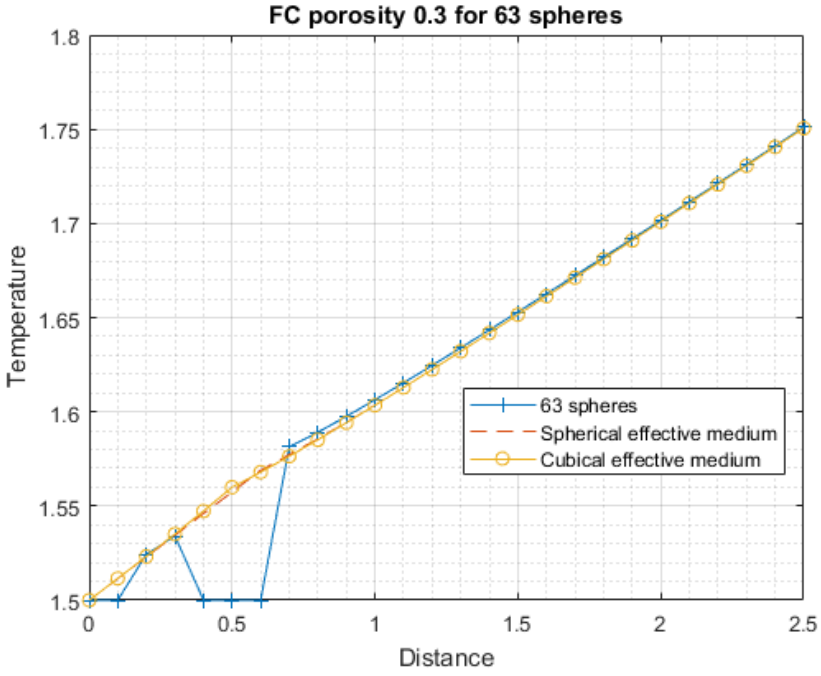

Figure 6.39: Plot of FCC cluster with porosity 0.3 for 63 pores vs spherical effective medium vs cubic effective medium

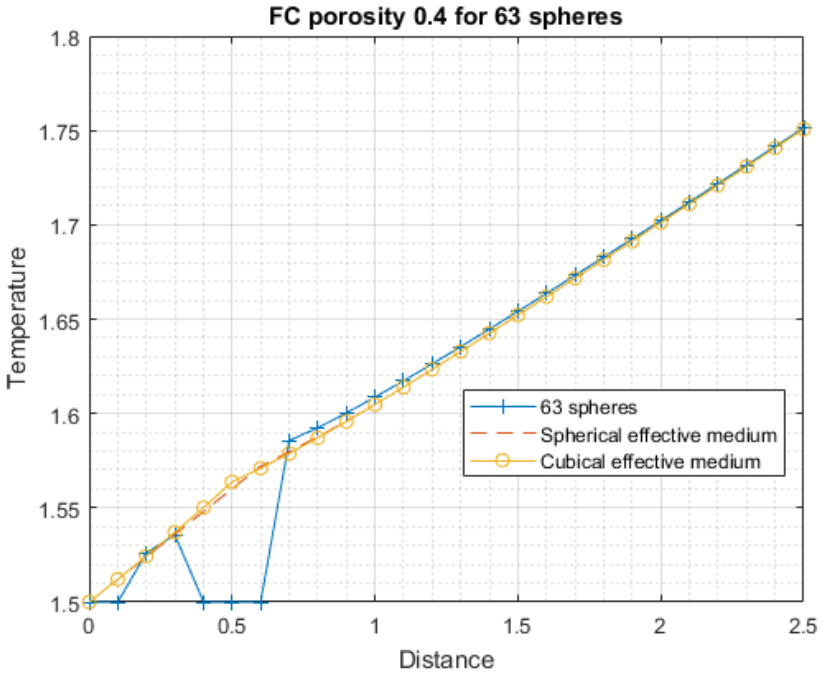

Figure 6.40: Plot of FCC cluster with porosity 0.4 for 63 pores vs spherical effective medium vs cubic effective medium

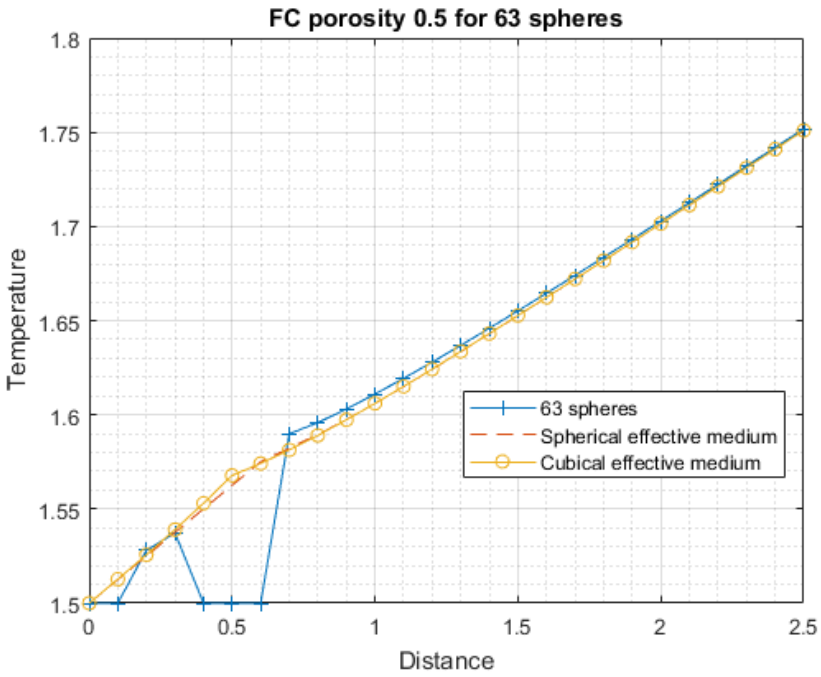

Figure 6.41: Plot of FCC cluster with porosity 0.5 for 63 pores vs spherical effective medium vs cubic effective medium

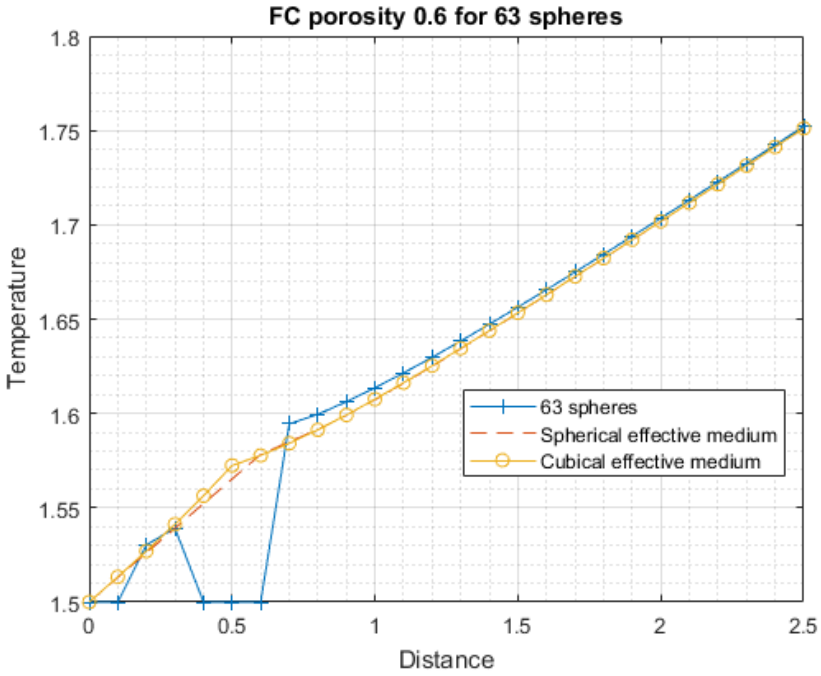

Figure 6.42: Plot of FCC cluster with porosity 0.6 for 63 pores vs spherical effective medium vs cubic effective medium

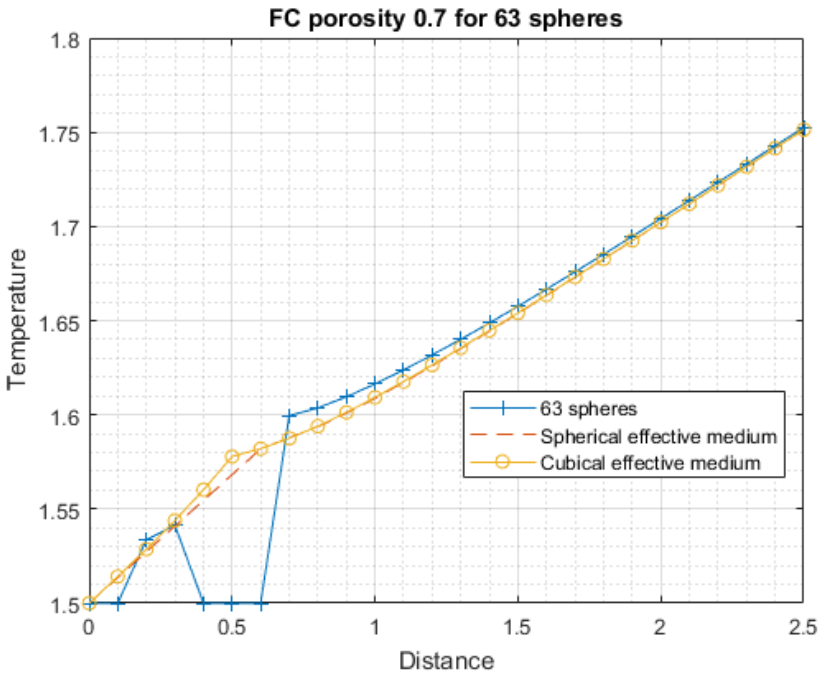

Figure 6.43: Plot of FCC cluster with porosity 0.7 for 63 pores vs spherical effective medium vs cubic effective medium

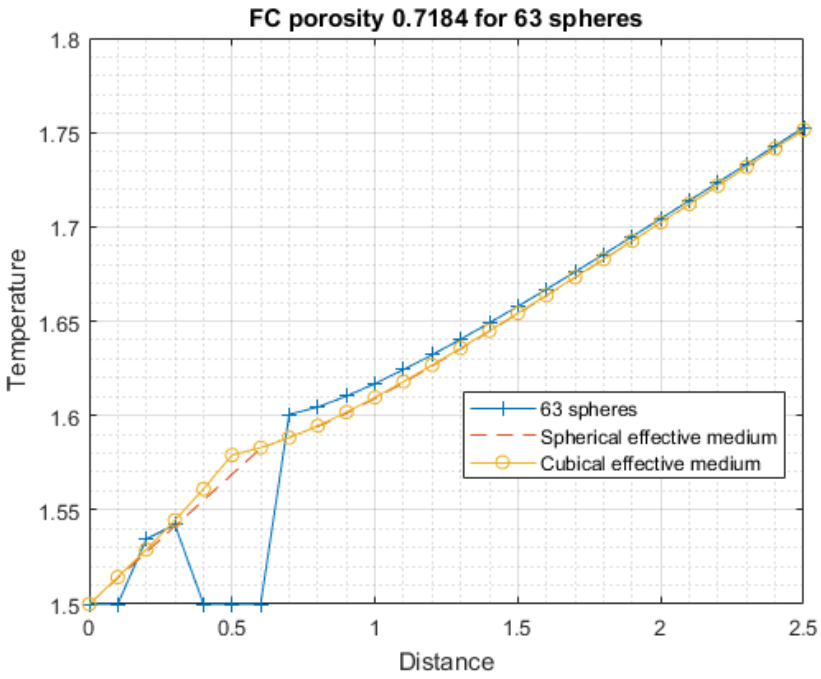

Figure 6.44: Plot of FCC cluster with porosity 0.7184 for 63 pores vs spherical effective medium vs cubic effective medium

6.3 Results on the effect of porosity on effective thermal conductivity

Effective thermal conductivity is calculated by using the equation

$$k_{eff} = \frac{\sum q}{\Delta T}, \tag{6.2}$$

where q is the average vertical heat flux at the top surface and ΔT is the temperature difference between top and bottom surface. The following tables shows the values of effective thermal conductivity for all three cases.

Table 6.1: Effective thermal conductivity for Case 1

Porosity	$k_{eff}(W/mK)$
0	1
0.05	0.9077
0.1	0.7997
0.15	0.7501
0.2	0.6773
0.25	0.6083
0.3	0.466
0.35	0.4971
0.4	0.4292

Table 6.2: Effective thermal conductivity for Case 2

Porosity	$k_{eff}(W/mK)$
0	1
0.1	0.8249
0.2	0.6694
0.3	0.5173

Table 6.3: Effective thermal conductivity for Case 3

Porosity	$k_{eff}(W/mK)$
0	1
0.05	0.9263
0.1	0.8589
0.15	0.7971

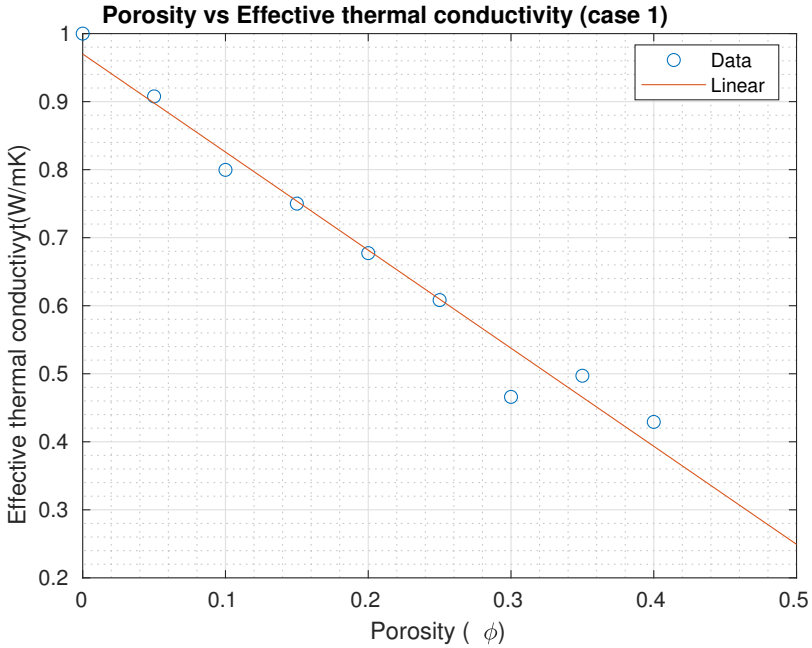

Figure 6.45: Linear fit for case 1

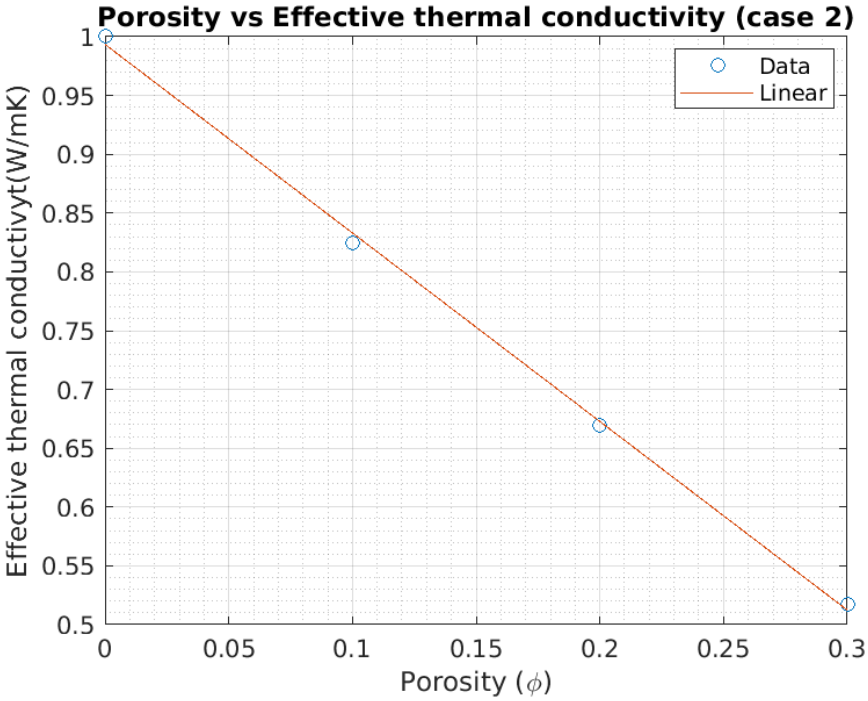

Figure 6.46: Linear fit for case 2

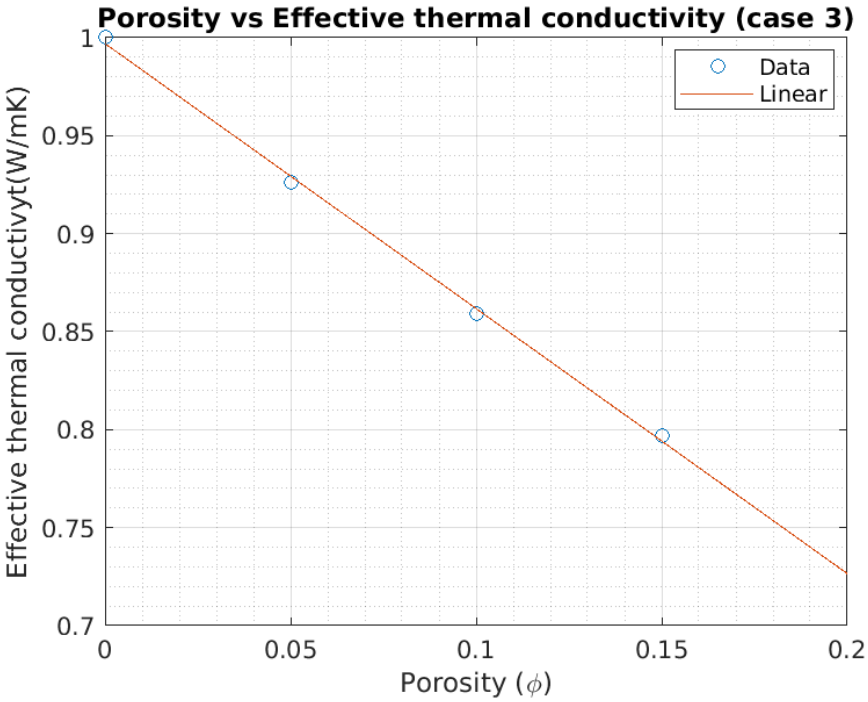

Figure 6.47: Linear fit for case 3

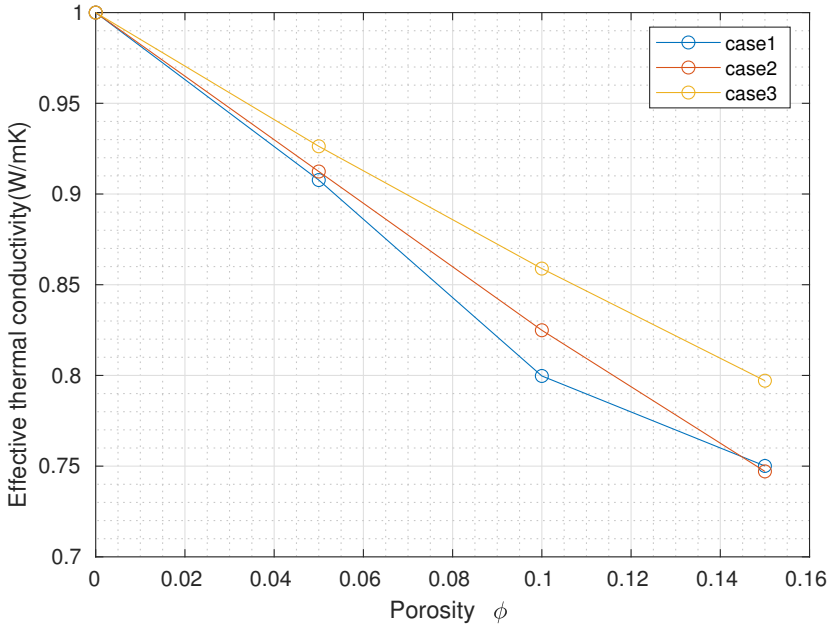

Figure 6.48: Comparison of three cases

The calculated effective thermal conductivities for all the three cases are plotted in Figs. 6.45-6.47. The plots clearly show a linear downward trend with increasing porosity. The results are plotted together in Fig. 6.48. As the figure shows, the effective thermal conductivities for cases 1 and 2 are approximately the same (the slight dip is very likely due to numerical issues) indicating that the effective thermal conductivity is a weak function of pore sizes for through-wall pores. On the other hand, the difference between case 1 and case 3 are more significant indicating that the effective thermal conductivity depends strongly on whether the pores are through-holes or part-through holes. This is a critical observation and points to the need for further studies on the dependence of effective thermal conductivity on the features of porous including size, shape, location, and orientation of the pores.

CHAPTER 7: CONCLUSIONS

In this study, effective thermal conductivity is defined. A two-phase composite material is considered with one phase representing the pores in the material. OOF3D was used to generate a FE model of a random micro-structure. OOF3D model was successfully imported into Abaqus to analyze and calculate effective thermal conductivity using steady-state heat-conduction.

Maxwell's modified methodology is also discussed in this study which accounts for interactions between the spherical particles. FEA models of the different cases are constructed with a cluster of spherical particles, equivalent spherical inhomgeneity and equivalent cubic inhomogeneity. Periodic arrangement of spherical particles in SC, BCC and FCC arrays are used for steady state FE analyses. Different porosities are considered in this study and the temperature for each case is plotted and compared for all the cases. At sufficiently large distances from the embedded structure, the effect of the inhomogeneities diminishes.

The voids in the isotropic material affects the effective thermal conductivity due to difference in material properties of the voids. Three cases are considered in this study to determine the relationship between the porosity and the effective thermal conductivity. Various cubic models are simulated with different size and geometry of pores. Steady-state heat-conduction analysis is carried out to find the average vertical heat flux to calculate effective thermal conductivity.

Linear regression models are plotted for all the cases. In each case, a linear drop is observed in the effective thermal conductivity. The first case has random arrangement of cylindrical pores through cubic model, the second one has cylindrical pores with different radii and the third has spherical pores embedded in the cubic model. The

comparison of all three cases shows that the effective thermal conductivity is lower for cylindrical pores than for the embedded spherical ones.

These approaches can be extended to transient heat conduction problems. However, a major hurdle is that the object oriented finite element analysis of scanned images is computationally intensive with the meshing and refining procedure taking significant amount of time. The method can be extended to non-porous composite materials with different phases. Maxwell's methodology can also be applied to random arrangements of spherical particles and non-spherical particles. Apart from that, it can also be useful in estimating other properties of materials based on small samples. Radiation effects can be considered to further refine the effective thermal conductivity estimates in porous materials.

REFERENCES

[1] S. Mogilevskaya, V. Kushch, O. Koroteeva, and S. Crouch, "Equivalent inhomogeneity method for evaluating the effective conductivities of isotropic particulate composites," *Journal of Mechanics of Materials and Structures*, vol. 7, no. 1, pp. 103–117, 2012.

[2] D. W. Hahn and M. N. Özisik, *Heat conduction*. John Wiley & Sons, 2012.

[3] Y.-H. Dong, C.-A. Wang, L.-F. Hu, and J. Zhou, "Numerical calculations of effective thermal conductivity of porous ceramics by image-based finite element method," *Frontiers of Materials Science*, vol. 6, no. 1, pp. 79–86, 2012.

[4] K. Schlichting, N. Padture, and P. Klemens, "Thermal conductivity of dense and porous yttria-stabilized zirconia," *Journal of materials science*, vol. 36, no. 12, pp. 3003–3010, 2001.

[5] V. R. Coffman, A. C. Reid, S. A. Langer, and G. Dogan, "Oof3d: An image-based finite element solver for materials science," *Mathematics and Computers in Simulation*, vol. 82, no. 12, pp. 2951–2961, 2012.

[6] L. N. McCartney and A. Kelly, "Maxwell's far-field methodology applied to the prediction of properties of multi-phase isotropic particulate composites," *Proceedings of the Royal Society A: Mathematical, Physical and Engineering Sciences*, vol. 464, no. 2090, pp. 423–446, 2007.

[7] C. Sun and R. Vaidya, "Prediction of composite properties from a representative volume element," *Composites Science and Technology*, vol. 56, no. 2, pp. 171–179, 1996.

[8] X. Chen and Y. Liu, "Square representative volume elements for evaluating the effective material properties of carbon nanotube-based composites," *Computational Materials Science*, vol. 29, no. 1, pp. 1–11, 2004.

[9] Z. Wang, A. Kulkarni, S. Deshpande, T. Nakamura, and H. Herman, "Effects of pores and interfaces on effective properties of plasma sprayed zirconia coatings," *Acta Materialia*, vol. 51, no. 18, pp. 5319–5334, 2003.

[10] K. Terada, T. Miura, and N. Kikuchi, "Digital image-based modeling applied to the homogenization analysis of composite materials," *Computational Mechanics*, vol. 20, no. 4, pp. 331–346, 1997.

[11] F. Liehr, T. Preusser, M. Rumpf, S. Sauter, and L. O. Schwen, "Composite finite elements for 3d image based computing," *Computing and visualization in science*, vol. 12, no. 4, pp. 171–188, 2009.

[12] B. Patzák and Z. Bittnar, "Design of object oriented finite element code," *Advances in Engineering Software*, vol. 32, no. 10-11, pp. 759–767, 2001.

[13] N. Chawla, B. Patel, M. Koopman, K. Chawla, R. Saha, B. Patterson, E. Fuller, and S. A. Langer, "Microstructure-based simulation of thermomechanical behavior of composite materials by object-oriented finite element analysis," *Materials Characterization*, vol. 49, no. 5, pp. 395–407, 2002.

[14] N. Takano, M. Zako, F. Kubo, and K. Kimura, "Microstructure-based stress analysis and evaluation for porous ceramics by homogenization method with digital image-based modeling," *International Journal of Solids and Structures*, vol. 40, no. 5, pp. 1225–1242, 2003.

[15] N. Michailidis, F. Stergioudi, H. Omar, and D. Tsipas, "An image-based reconstruction of the 3d geometry of an al open-cell foam and fem modeling of the material response," *Mechanics of Materials*, vol. 42, no. 2, pp. 142–147, 2010.

[16] N. K. Sharma, R. Misra, and S. Sharma, "Modeling of thermal expansion behavior of densely packed al/sic composites," *International Journal of Solids and Structures*, vol. 102, pp. 77–88, 2016.

[17] E. Celik and O. Sarikaya, "The effect on residual stresses of porosity in plasma sprayed mgo–zro2 coatings for an internal combustion diesel engine," *Materials Science and Engineering: A*, vol. 379, no. 1-2, pp. 11–16, 2004.

[18] K. Anish, K. Krishnakumar, and T. Ratnish, "Numerical method to determine effective thermal conductivity of perforated plate matrix heat exchanger surfaces and its experimental validation," *Int Đ of Sci and Eng Res*, vol. 5, no. 5, pp. 1079–1084, 2014.

[19] S.-Y. Chung, D. Stephan, M. A. Elrahman, and T.-S. Han, "Effects of anisotropic voids on thermal properties of insulating media investigated using 3d printed samples," *Construction and Building Materials*, vol. 111, pp. 529–542, 2016.

[20] S. G. Mogilevskaya, S. L. Crouch, H. K. Stolarski, and A. Benusiglio, "Equivalent inhomogeneity method for evaluating the effective elastic properties of unidirectional multi-phase composites with surface/interface effects," *International Journal of Solids and Structures*, vol. 47, no. 3-4, pp. 407–418, 2010.

[21] S. G. Mogilevskaya, V. I. Kushch, H. K. Stolarski, and S. L. Crouch, "Evaluation of the effective elastic moduli of tetragonal fiber-reinforced composites based on maxwell's concept of equivalent inhomogeneity," *International Journal of Solids and Structures*, vol. 50, no. 25-26, pp. 4161–4172, 2013.

[22] O. Koroteeva, S. Mogilevskaya, S. Crouch, and E. Gordeliy, "A computational technique for evaluating the effective thermal conductivity of isotropic porous materials," *Engineering analysis with boundary elements*, vol. 34, no. 9, pp. 793–801, 2010.

[23] V. I. Kushch and S. G. Mogilevskaya, "On convergence of the generalized maxwell scheme: conductivity of composites containing cubic arrays of spherical particles," *Philosophical Magazine Letters*, vol. 96, no. 10, pp. 392–401, 2016.

[24] S. G. Mogilevskaya and S. L. Crouch, "Combining maxwell's methodology with the bem for evaluating the two-dimensional effective properties of composite and micro-cracked materials," *Computational Mechanics*, vol. 51, no. 4, pp. 377–389, 2013.

[25] W. Węglewski, M. Basista, M. Chmielewski, and K. Pietrzak, "Modeling of thermally induced damage in the processing of cr–al2o3 composites," *Composites Part B: Engineering*, vol. 43, no. 2, pp. 255–264, 2012.

[26] L. McCartney, "Maxwell's far-field methodology predicting elastic properties of multiphase composites reinforced with aligned transversely isotropic spheroids," *Philosophical Magazine*, vol. 90, no. 31-32, pp. 4175–4207, 2010.

[27] L. Germanovich and A. Dyskin, "Virial expansions in problems of effective characteristics. 1. general concepts," *Mechanics of composite materials*, vol. 30, no. 2, pp. 157–167, 1994.

[28] R. McPhedran and D. McKenzie, "The conductivity of lattices of spheres i. the simple cubic lattice," *Proceedings of the Royal Society of London. A. Mathematical and Physical Sciences*, vol. 359, no. 1696, pp. 45–63, 1978.

[29] D. R. McKenzie, R. McPhedran, and G. Derrick, "The conductivity of lattices of spheres-ii. the body centred and face centred cubic lattices," *Proceedings of the Royal Society of London. A. Mathematical and Physical Sciences*, vol. 362, no. 1709, pp. 211–232, 1978.

[30] A. S. Sangani and A. Acrivos, "The effective conductivity of a periodic array of spheres," *Proceedings of the Royal Society of London. A. Mathematical and Physical Sciences*, vol. 386, no. 1791, pp. 263–275, 1983.

[31] I. Chan Kim and S. Torquato, "Effective conductivity of suspensions of hard spheres by brownian motion simulation," *Journal of applied physics*, vol. 69, no. 4, pp. 2280–2289, 1991.

[32] E. Gordeliy, S. L. Crouch, and S. G. Mogilevskaya, "Transient heat conduction in a medium with multiple spherical cavities," *International Journal for Numerical Methods in Engineering*, vol. 77, no. 6, pp. 751–775, 2009.

[33] S. Mogilevskaya and D. Nikolskiy, "The shape of maxwell's equivalent inhomogeneity and 'strange' properties of regular polygons and other symmetric domains," *The Quarterly Journal of Mechanics and Applied Mathematics*, vol. 68, no. 4, pp. 363–385, 2015.